concomitantly with the induction of occludin mRNA, the expression of occludin protein was examined in TR-BBB13 cells for 8 days (Figs 1b and c). A single band at 65 kDa was detected in TR-BBB13 cells, corresponding in size to the bands from rat brain and isolated rat brain capillary used as positive controls, whereas no band was detected in TR-AST4 cells (Fig. 1b). Moreover, TR-AST4 cells did not express occludin mRNA (data not shown). The ratio of occludin to β-actin density in co-culture was 1.77-fold greater than that in single culture (Fig. 1c). The TEER in TR-BBB13 cells was unchanged by co-culture (106 ± 2 and 106 ± 1 ohm cm^2) compared with single culture (103 ± 1 and 109 ± 2 ohm cm^2) for 6 and 8 days, respectively.

Induction of occludin mRNA in TR-BBB13 cells by treatment with AST-CM or PCT-CM

To determine the regulatory effects of soluble factors secreted from TR-AST4 and TR-PCT1 cells, the expressional change of occludin and JAM mRNAs was examined in TR-BBB13 cells treated with AST-CM or PCT-CM (Fig. 2). The occludin mRNA level in TR-BBB13 cells was significantly increased by treatment with both CMs (Fig. 2a). Following treatment with AST-CM, the occludin mRNA level was increased in a concentration-dependent manner, and the occludin mRNA level was increased and reached a plateau at two-fold concentrated CM in the case of PCT-CM treatment. In contrast, the JAM mRNA level was not significantly changed by the presence of one- to five-fold concentrated AST-CM or PCT-CM compared with each control medium (Fig. 2b).

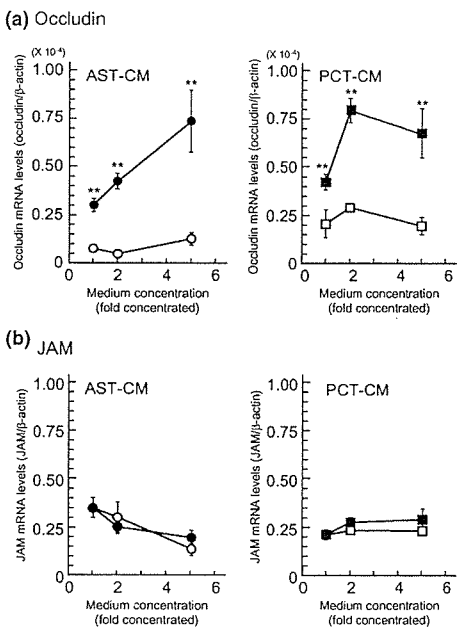

Fig. 2 Induction of occludin mRNA in TR-BBB13 cells by treatment with AST-CM or PCT-CM. Effects of AST-CM (●) or PCT-CM (■) on the occludin (a) and JAM (b) mRNA levels in TR-BBB13 cells for 24 h. ○, control medium for AST-CM; □, control medium for PCT-CM. The occludin and JAM mRNA levels were determined by quantitative real-time PCR analysis. Each point represents the mean ± SEM ($n = 3$). Each mRNA expression level was normalized with respect to the β-actin mRNA expression. $^{**}p < 0.01$, significantly different from the control.

Regulation of occludin mRNA by angiopoietin-1, VEGF and TGF-β1

The effects of 24-h treatment of angiopoietin-1, VEGF and TGF-β1 on the occludin mRNA level were examined in TR-BBB13 cells (Fig. 3). The occludin mRNA level significantly increased following treatment with > 1.0 ng/mL angiopoietin-1 compared with non-treated cells (1.73-fold by 1.0 ng/mL; 1.76-fold by 10 ng/mL; 2.09-fold by 100 ng/mL; 2.20-fold by 500 ng/mL) (Fig. 3a). Conversely, the occludin mRNA level was significantly reduced following the addition of VEGF (1.0 ng/mL, by 25.9%; 10 ng/mL, by 35.9%) or TGF-β1 (0.1 ng/mL, by 17.1%; 1.0 ng/mL, by

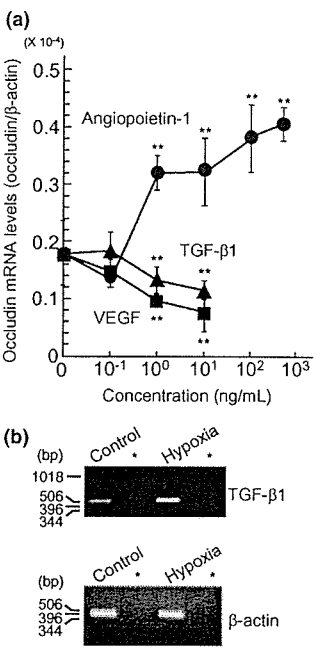

Fig. 3 Effects of angiopoietin-1, VEGF and TGF-β1 on the occludin mRNA level in TR-BBB13 cells (a) and effect of hypoxia on the expression level of TGF-β1 mRNA in TR-AST4 cells (b). (a) Effects of angiopoietin-1 (●), TGF-β1 (▲) and VEGF (■) on the occludin mRNA level in TR-BBB13 cells for 24 h. The occludin mRNA levels were determined by quantitative real-time PCR analysis. Each mRNA expression level was normalized with respect to the β-actin mRNA expression. $^{**}p < 0.01$, significantly different from the control. (b) RT-PCR analysis of TGF-β1 and β-actin in TR-AST4 cells under normal conditions (control) and 24-h hypoxic conditions. *Respective RT(–) for left-hand lane.

46.3%; 10 ng/mL, by 57.4%) for 24 h (Fig. 3a). The JAM mRNA level remained unchanged under any of these conditions (data not shown). To clarify the involvement of TGF-β1 under pathophysiological conditions, the effect of hypoxic conditions on the mRNA expression level of TGF-β1 was determined in TR-AST4 cells by RT-PCR analysis. The mRNA expression of TGF-β1 was increased in TR-AST4 cells following a 24-h period of hypoxia as shown in Fig. 3(b).

Effect of anti-angiopoietin-1 antibody on induction of occludin mRNA in TR-BBB13 cells by AST-CM and PCT-CM

To clarify the contribution of angiopoietin-1 to the induction of occludin mRNA in TR-BBB13 cells by AST-CM and PCT-CM, angiopoietin-1 activity was neutralized with anti-angiopoietin-1 antibody. The induction of occludin mRNA after 24-h treatment with 10 ng/mL angiopoietin-1 was reduced by 79.0% following pre-treatment with the antibody, indicating that the antibody possesses angiopoietin-1-neutralizing activity (Fig. 4a). The occludin mRNA level was not inhibited in TR-BBB13 cells by AST-CM pre-treated with the antibody (Fig. 4b). In contrast, following stimulation with one-, two- and five-fold concentrated PCT-CM pre-treated with anti-angiopoietin-1 antibody, the occludin mRNA level was inhibited by 62.6, 61.4 and 45.1%, respectively (Fig. 4c).

Induction of occludin mRNA in TR-BBB13 cells by fractionated AST-CMs

To determine the approximate molecular weight of TR-AST4 cell-derived soluble factors regulating the occludin mRNA level, a study using fractionated AST-CMs was performed (Fig. 5). The occludin mRNA level was increased by 2.50-, 1.99- and 2.44-fold following treatment with AST-CM (> 10-kDa CM), 30- to 50-kDa and 50- to 100-kDa AST-CM, respectively (Fig. 5a). In contrast, the JAM mRNA level in TR-BBB13 cells was not changed by any of the fractionated AST-CMs (Fig. 5b).

Identification of angiopoietin-1 secretion from TR-PCT1 cells

The mRNA expression of angiopoietin-1 was detected in TR-PCT1 cells at the same level as in rat lung, used as a positive control, but was not detected in TR-AST4 cells (Fig. 6a). Western blot analysis was performed for PCT-CM with or without reducing agents in order to clarify whether angiopoietin-1 secreted from TR-PCT1 cells forms a complex via disulfide bonds, as reported previously (Procopio *et al.* 1999) (Fig. 6b). Several bands at >250 kDa were detected in PCT-CM under non-reducing conditions. Recombinant human angiopoietin-1, used as a positive control, was detected at >250 kDa under non-reducing conditions. The reducing conditions led to a reduction in the apparent molecular weight of bands. The shifted band was single, and detected at 65 and 75 kDa in PCT-CM and recombinant human angiopoietin-1, respectively.

Expression and tyrosine phosphorylation of Tie-2 in TR-BBB13 cells treated with PCT-CM or angiopoietin-1

Western blot analysis revealed that Tie-2 protein, a tyrosine kinase receptor of angiopoietin-1, was expressed in TR-BBB13 cells and had the same molecular weight as that expressed in rat brain and isolated rat brain capillary, used as

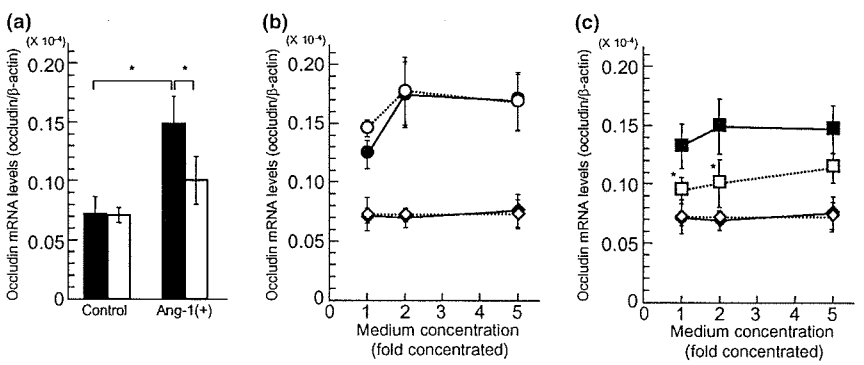

Fig. 4 Effect of anti-angiopoietin-1 antibody on occludin induction by treatment with AST-CM or PCT-CM. (a) TR-BBB13 cells were cultured in the presence [Ang-1(+)] or absence (control) of recombinant human angiopoietin-1 pre-treated with anti-angiopoietin-1 antibody (open columns) or normal rabbit IgG (black columns). (b) TR-BBB13 cells were cultured with AST-CM (circle symbols) or control medium (diamond symbols) pre-treated with anti-angiopoietin-1 antibody (open symbols) or normal rabbit IgG (closed symbols). (c) TR-BBB13 cells were cultured with PCT-CM (square symbols) or control medium (diamond symbols) pre-treated with anti-angiopoietin-1 antibody (open symbols) or normal rabbit IgG (closed symbols). The occludin mRNA levels were determined by quantitative real-time PCR analysis. Each column or point represents the mean ± SEM ($n = 3$). Each mRNA expression level was normalized with respect to the β-actin mRNA expression. $^*p < 0.05$, significantly different from the control.

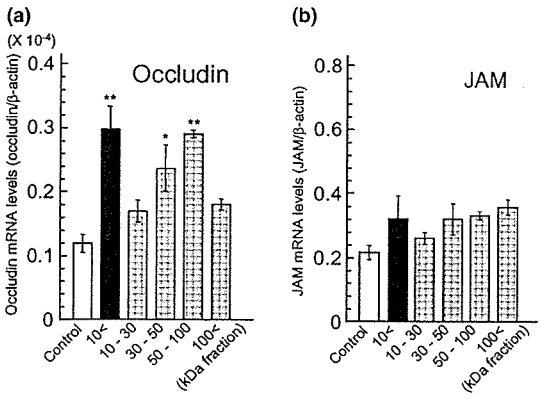

Fig. 5 Effects of fractionated AST-CMs on the occludin (a) and JAM (b) mRNA levels in TR-BBB13 cells. TR-BBB13 cells were cultured with fractionated AST-CM [> 10 (black column), 10–30, 30–50, 50–100 and > 100 kDa fractionated CM (gray columns)] for 24 h. Open column indicates treatment with control medium (serum-free). The occludin and JAM mRNA levels were determined by quantitative real-time PCR analysis. Each column represents the mean ± SEM ($n = 3$). Each mRNA expression level was normalized with respect to the β-actin mRNA expression. $^{**}p < 0.01$, $^{*}p < 0.05$, significantly different from the control.

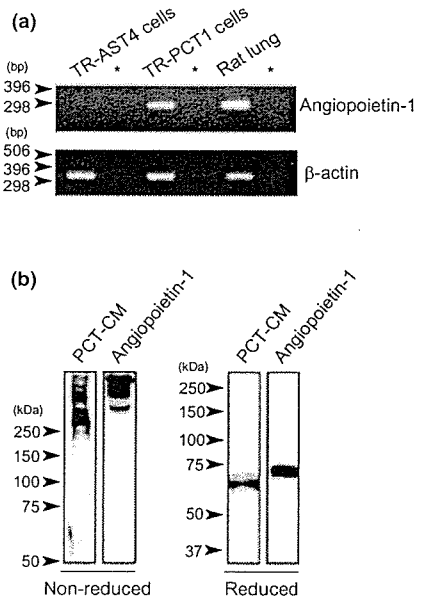

Fig. 6 Secretion of angiopoietin-1 from TR-PCT1 cells. (a) RT-PCR analysis of angiopoietin-1 and β-actin mRNA in TR-AST4 cells, TR-PCT1 cells and rat lung as a positive control. *Respective RT(–) for left-hand lane. (b) Western blot analysis of angiopoietin-1 in PCT-CM in the presence (Reduced) or absence (Non-reduced) of reducing agents (dithiothreitol and 2-mercaptoethanol). Recombinant human angiopoietin-1 was used as a positive control.

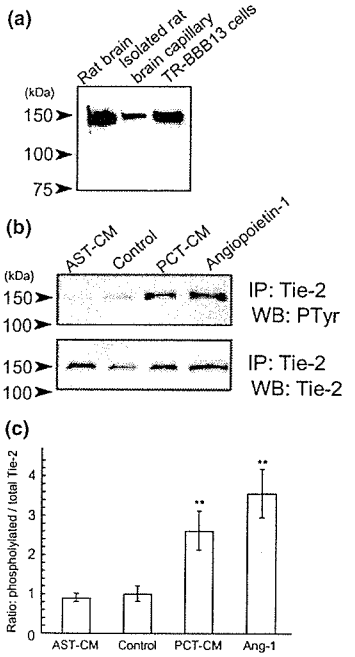

Fig. 7 Expression of Tie-2 (a) and effects of PCT-CM and recombinant human angiopoetin-1 on Tie-2 tyrosine phosphorylation (b and c) in TR-BBB13 cells. (a) Western blot analysis of Tie-2 in rat brain and isolated rat brain capillary as positive controls, and TR-BBB13 cells. (b) TR-BBB13 cells were cultured with two-fold concentrated AST-CM, PCT-CM or 300 ng/mL recombinant human angiopoietin-1. After 24 h, cellular extracts from the treated cells were immunoprecipitated (IP) with anti-Tie-2 antibody followed by western blot analysis (WB) with anti-PTyr antibody (upper) or anti-Tie-2 antibody (lower). A typical result from five experiments is shown. (c) The ratio of tyrosine phosphorylated Tie-2 density to total Tie-2 density. Ang-1, recombinant human angiopoietin-1. Each column represents the mean ± SEM ($n = 5$). $^{**}p < 0.01$, significantly different from non-treated cells (control).

positive controls (Fig. 7a). The tyrosine phosphorylation of Tie-2 protein after 24-h treatment with two-fold concentrated PCT-CM was examined by immunoprecipitation and western blot analyses (Figs 7b and c). The immunoprecipitated Tie-2 protein was electrophoresed and immunoblotted with anti-PTyr antibody. As shown in Fig. 7(b) (upper panel), the tyrosine phosphorylation of Tie-2 protein increased in TR-BBB13 cells treated with PCT-CM or 300 ng/mL recombinant human angiopoietin-1 (a positive control) compared with that in non-treated TR-BBB13 cells. In contrast, the phosphorylated Tie-2 protein was unchanged in TR-BBB13 cells treated with AST-CM. The amount of Tie-2 protein was not affected by any of the treatment conditions (Fig. 7b, lower panel). The ratio of tyrosine phosphorylated Tie-2 to total Tie-2 density in TR-BBB13 cells treated with AST-CM, PCT-CM or recombinant human angiopoietin-1 was, respectively, 0.89-, 2.60- or 3.55-fold greater than that in non-treated TR-BBB13 cells (Fig. 7c).

Discussion

The present study demonstrated that soluble factors secreted from TR-AST4 cells and TR-PCT1 cells induced occludin expression in TR-BBB13 cells. Angiopoietin-1 in PCT-CM predominantly induced occludin expression via Tie-2 tyrosine phosphorylation in TR-BBB13 cells, and was secreted from TR-PCT1 cells as a multimeric disulfide-linked complex (an active form of angiopoietin-1), but not secreted from TR-AST4 cells. This is the first direct evidence concerning the signaling pathway for occludin induction from brain pericytes to BCECs.

The amounts of occludin mRNA and protein were increased in TR-BBB13 cells in transfilter co-culture with cells of the type II astrocyte cell line, TR-AST4 cells (Fig. 1). Type II astrocytes appear to exist in the mature CNS, corresponding to mature fibrous astrocytes mainly localized in white matter (Miller and Raff 1984). This result suggests that fibrous astrocytes ensheathing microvessels at least play some role in maintaining occludin expression at the BBB, mediated by releasing factors and/or a direct contact effect. The concentration-dependent induction of occludin mRNA by AST-CM revealed that soluble factors secreted from TR-AST4 cells induced the occludin gene expression in TR-BBB13 cells (Fig. 2). Direct contact with TR-AST4 cells was also possibly involved in the occludin induction in TR-BBB13 cells, since the membrane pore size (3.0 μm) of the cell culture insert used in the present study was the same as that used in the report in which direct cell-to-cell contact was demonstrated by electron microscopic analysis (Hayashi *et al.* 1997). Moreover, PCT-CM increased the occludin mRNA level, as well as AST-CM (Fig. 2), suggesting that soluble factors secreted from both type II astrocytes and brain pericytes contribute to the induction of occludin expression at the BBB.

Following treatment with angiopoietin-1, the occludin mRNA level was increased in TR-BBB13 cells (Fig. 3a). The expression of occludin mRNA tends to increase in the range of 1–500 ng/mL angiopoietin-1 treatment, and its mRNA level of 500 ng/mL was significantly different from that of 1 ng/mL. This trend is compatible with the reported K_D value of angiopoietin-1 for Tie-2 (about 3 nM, it is calculated as 173 ng/mL when the molecular weight of angiopoietin-1 is 57.7 kDa) (Maisonpierre *et al.* 1997). This result raised the possibility that the occludin gene induction by AST-CM and PCT-CM was partly mediated by angiopoietin-1. The inhibition study using anti-angiopoietin-1-neutralizing antibody revealed that angiopoietin-1 is mainly responsible for the occludin-inducing activity produced by PCT-CM, as shown in Fig. 4(c). Moreover, RT-PCR analysis confirmed that TR-PCT1 cells expressed angiopoietin-1 mRNA (Fig. 6a). Therefore, angiopoietin-1 is suggested to be the predominant occludin-inducing factor secreted from brain pericytes.

In contrast, occludin induction by AST-CM was not inhibited by treatment with angiopoietin-1-neutralizing antibody (Fig. 4b), and TR-AST4 cells did not express angiopoietin-1 mRNA (Fig. 6a). These results indicate that the soluble factors inducing occludin mRNA in AST-CM are different from angiopoietin-1. The absence of angiopoietin-1 in TR-AST4 cells reflects that in mature astrocytes; it has been reported that the mRNA expression level of angiopoietin-1 in astrocytes is low after 3 weeks after birth (Acker *et al.* 2001). During the present study, Lee *et al.* reported that angiopoietin-1 secreted from astrocytes under reoxygenated conditions induces occludin expression in the developing BBB (Lee *et al.* 2003). Taken together, these results suggest that pericyte-derived angiopoietin-1 and astrocyte-derived undefined factors act to induce occludin expression in the mature BBB. Moreover, angiopoietin-1 seems to be a crucial factor for occludin induction at both the mature and developing BBB, although the cell types secreting angiopoietin-1 seem to change with aging.

The fractionated AST-CM study revealed that the 30- to 50-kDa and 50- to 100-kDa fractions contain factors involved in inducing occludin expression (Fig. 5), although these factors remained undefined in the present study. Interleukin-15 and prolactin have been reported to induce occludin expression in epithelial cells (Stelwagen *et al.* 1999; Nishiyama *et al.* 2001). However, the size of the secreted interleukin-15 and prolactin is less than 20 kDa. Accordingly, unknown factors other than interleukin-15 and prolactin induce occludin expression in TR-AST4 cells. Identification of the occludin-inducing factors using AST-CM should provide a better understanding of the physiological regulators of expression of occludin secreted from type II astrocytes.

VEGF and TGF-β1 are known to be increased in the brain in various neurodegenerative diseases (Kalaria *et al.* 1998; Lesne *et al.* 2002). Following treatment with VEGF, the occludin mRNA level was reduced in a concentration-dependent manner in TR-BBB13 cells (Fig. 3a). This result is consistent with a previous report on primary bovine BCECs (Wang *et al.* 2001). TGF-β1 also reduced the occludin mRNA level in a concentration-dependent manner in TR-BBB13 cells (Fig. 3a). This suggests that the BBB disruption induced by TGF-β1 occurs at least partly by a reduction in occludin. The TGF-β1 mRNA level was enhanced in TR-AST4 cells during a 24-h period of hypoxia (Fig. 3b). This was the case for the *in vivo* response of astrocytes under ischemic conditions (Knuckey *et al.* 1996), suggesting that type II astrocytes may reduce occludin expression in BCECs under ischemic conditions by producing TGF-β1. In the light of these findings, the occludin expression is regulated by astrocyte- and pericyte-derived factors under physiological and pathophysiological conditions (Fig. 8).

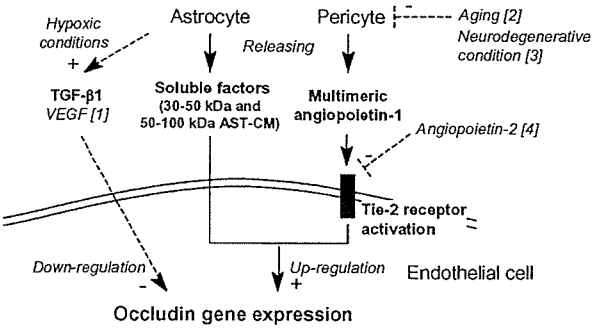

Fig. 8 Postulated mechanism of occludin gene regulation by astrocytes and pericytes for maintaining the adult BBB. [1], Kalaria *et al.* (1998); [2], Heinsen and Heinsen (1983); [3], Verbeek *et al.* (1997); [4], Maisonpierre *et al.* (1997).

JAM expression was unchanged by TR-AST4 cells and TR-PCT1 cells (Figs 1 and 2). This suggests that regulation of JAM expression at the BBB is not regulated by type II astrocytes and brain pericytes, unlike that of occludin. JAM plays a role in inflammatory transmigration of leukocytes as a ligand of integrins (Ostermann *et al.* 2002). The function of JAM in leukocyte migration may not be influenced by microenvironmental stimuli such as astrocytes and pericytes, VEGF and TGF-β1. Although the concentrated-CM tends to reduce JAM mRNA levels in the left panel of Fig. 2(b), it is not significantly different from non-concentrated-CM. The concentrated-CM would not affect the JAM mRNA in TR-BBB13 cells because other concentrated-CMs did not change JAM or occludin mRNA levels from one- to five-fold concentrated-CM (Fig. 2).

Induction of occludin expression in brain microvessels possibly enhances the tightness of TJs, since overexpression of occludin in MDCK cells has been reported to elevate their TEER (McCarthy *et al.* 1996). However, the TEER in TR-BBB13 cells was unchanged by the induction of occludin expression following the transfilter co-culture. Claudin-5 is involved in TJ formation at the BBB, and the BBB of the corresponding knock-out mouse showed a loss of tightness for solutes with a permeability under 800 Da (Nitta *et al.* 2003). Therefore, it is conceivable that TJ formation at the BBB is necessary for claudin-5 as well as occludin. Indeed, the expression level of claudin-5 mRNA in TR-BBB13 cells was very low compared with that of occludin mRNA (data not shown).

The multimeric character of the angiopoietin-1 secreted from pericytes was demonstrated using TR-PCT1 cells (Fig. 6). The 65-kDa protein in PCT-CM is possibly monomeric angiopoietin-1 since it is the same size as recombinant rat angiopoietin-1 reported previously (Iizasa *et al.* 2002). The size-difference between PCT-CM (65 kDa) and recombinant human angiopoietin-1 (75 kDa) is possibly due to the degree of glycosylation exhibited by difference in species and host cells. The low mobility of the bands detected under non-reducing conditions indicates that angiopoietin-1 forms a disulfide-linked complex, mostly larger than tetrameric. Tetrameric angiopoietin-1 has been recently reported to be the minimal size required for Tie-2 activation (Davis *et al.* 2003). Therefore, a multimeric complex of angiopoietin-1 endogenously secreted from TR-PCT1 cells is very likely to activate the Tie-2 receptor.

Tyrosine phosphorylation of Tie-2 in TR-BBB13 cells was induced by PCT-CM as shown in Fig. 7. Therefore, the signaling pathway from angiopoietin-1 multimers in PCT-CM to occludin mRNA induction through Tie-2 autophosphorylation is clearly demonstrated. The p85 subunit of phosphatidylinositol 3-kinase (PI3-kinase), the adaptor proteins Grb2, Grb7 and Grb14, and the protein tyrosine phosphatase Shp2 can interact with Tie-2 in a phosphotyrosine-dependent manner (Jones *et al.* 1999), and are potential downstream molecules of Tie-2. Among these molecules, PI3-kinase has been reported to influence TJ function although this is controversial. It has been reported that PI3-kinase activation increases the amount of occludin localized at the cell surface (Little *et al.* 2003) although this, conversely, leads to TJ disruption (Woo *et al.* 1999). Further studies are needed to elucidate the signal molecules involved in occludin induction following the angiopoietin-1/Tie-2 signal.

The present study suggests that the attenuation or inhibition of the angiopoitin-1/Tie-2 pathway between BCECs and brain pericytes leads to dysfunction of the TJs at the BBB in disease. There are two possible ways of modifying the pathway; one is changing the secretion of angiopoietin-1 from pericytes, and the other is inhibition of the interaction between angiopoietin-1 and Tie-2 (Fig. 8). As far as the latter is concerned, angiopoietin-2 is known to suppress angiopoietin-1 activity as an antagonist of Tie-2 (Maisonpierre *et al.* 1997). In PCT-CM, angiopoietin-1 is possibly a dominant factor compared with angiopoietin-2, since angiopoietin-1-dependent occludin induction is seen following treatment with PCT-CM (Fig. 4c). The expression level of angiopoietin-2 is induced under hypoxic conditions in brain, whereas angiopoietin-1 expression is unchanged (Mandriota *et al.* 2000). Therefore, it is conceivable that angiopoietin-2 affects occludin expression under pathophysiological conditions by modifying the angiopoietin-1/Tie-2 pathway. The occludin regulation by angiopoietin-1 and angiopoietin-2 is very important for a better understanding of the regulation of TJs at the BBB. Mouse angiopoietin-3 and human angiopoietin-4, other members of the angiopoietin family, are also ligands of Tie-2 (Valenzuela *et al.* 1999). There is little possibility that angiopoietin-3 and angiopoietin-4 modulate the TJ function at the BBB because their expression was not detected in the brain (Valenzuela *et al.* 1999), whereas the contribution of angiopoietin-3 and angiopoietin-4 to occludin regulation is still unknown.

Pericyte degeneration seen with aging (Heinsen and Heinsen 1983; Peters *et al.* 1991) and in neurodegenerative conditions (Verbeek *et al.* 1997) is associated with increased permeability of the BBB. Moreover, it has been suggested that the reduction of the occludin content at the rat BBB takes place in an age-dependent manner (Mooradian *et al.* 2003). The findings of the present study indicate that one of the mechanisms of occludin reduction would be a decrease in angiopoietin-1 from pericytes, and this may partly explain the increased permeability following pericyte loss (Fig. 8).

In conclusion, *in vitro* BBB model studies have demonstrated that soluble factors (the molecular weight range of candidates is 30–100 kDa) secreted from type II astrocytes and multimeric angiopoietin-1, activating the Tie-2 receptor via tyrosine phosphorylation, secreted from pericytes induce occludin expression. In contrast, VEGF and TGF-β1, the mRNA of which was up-regulated in type II astrocytes following hypoxic treatment, reduced occludin mRNA. These findings provide important information about the molecular mechanism of TJ regulation based on paracrine interactions between BECEs, and astrocytes and pericytes under both physiological and pathophysiological conditions, and should help in the design of molecules to block TJ disruption and, thereby, protect the CNS.

Acknowledgements

The authors wish to thank Drs K. Tetsuka, T. Asashima and Messrs. H. Iizasa, T. Kondo for valuable discussions and Ms. N. Funayama for secretarial assistance. This study was supported, in part, by a Grant-in-Aid for Scientific Research, and a 21st Century Center of Excellence (COE) Program from Japan Society for the Promotion of Science. It was also supported in part by the Tokyo Biochemical Research Foundation and the Industrial Technology Research Grant Program in '00 from the New Energy and the Industrial Technology Development Organization (NEDO) of Japan.

References

Abbott N. J. (2002) Astrocyte–endothelial interactions and blood–brain barrier permeability. *J. Anat.* **200**, 629–638.

Acker T., Beck H. and Plate K. H. (2001) Cell type specific expression of vascular endothelial growth factor and angiopoietin-1 and -2 suggests an important role of astrocytes in cerebellar vascularization. *Mech. Dev.* **108**, 45–57.

Asashima T., Iizasa H., Terasaki T., Hosoya K., Tetsuka K., Ueda M., Obinata M. and Nakashima E. (2002) Newly developed rat brain pericyte cell line, TR-PCT1, responds to transforming growth factor-beta1 and beta-glycerophosphate. *Eur. J. Cell Biol.* **81**, 145–152.

Asashima T., Iizasa H., Terasaki T. and Nakashima E. (2003) Rat brain pericyte cell lines expressing beta2-adrenergic receptor, angiotensin II receptor type 1A, klotho, and CXCR4 mRNAs despite having endothelial cell markers. *J. Cell Physiol.* **197**, 69–79.

Davies D. C. (2002) Blood–brain barrier breakdown in septic encephalopathy and brain tumours. *J. Anat.* **200**, 639–646.

Davis S., Aldrich T. H., Jones P. F. *et al.* (1996) Isolation of angiopoietin-1, a ligand for the TIE2 receptor, by secretion-trap expression cloning. *Cell* **87**, 1161–1169.

Davis S., Papadopoulos N., Aldrich T. H. *et al.* (2003) Angiopoietins have distinct modular domains essential for receptor binding, dimerization and superclustering. *Nat. Struct. Biol.* **10**, 38–44.

Furuse M., Hirase T., Itoh M., Nagafuchi A., Yonemura S. and Tsukita S. (1993) Occludin: a novel integral membrane protein localizing at tight junctions. *J. Cell Biol.* **123**, 1777–1788.

Gaillard P. J., van der Sandt I. C., Voorwinden L. H., Vu D., Nielsen J. L., de Boer A. G. and Breimer D. D. (2000) Astrocytes increase the functional expression of P-glycoprotein in an in vitro model of the blood–brain barrier. *Pharm. Res.* **17**, 1198–1205.

Hayashi Y., Nomura M., Yamagishi S., Harada S., Yamashita J. and Yamamoto H. (1997) Induction of various blood–brain barrier properties in non-neural endothelial cells by close apposition to co-cultured astrocytes. *Glia* **19**, 13–26.

Heinsen H. and Heinsen Y. L. (1983) Cerebellar capillaries. Qualitative and quantitative observations in young and senile rats. *Anat. Embryol.* **168**, 101–116.

Hirase T., Staddon J. M., Saitou M., Ando-Akatsuka Y., Itoh M., Furuse M., Fujimoto K., Tsukita S. and Rubin L. L. (1997) Occludin as a possible determinant of tight junction permeability in endothelial cells. *J. Cell Sci.* **110**, 1603–1613.

Hosoya K., Tetsuka K., Nagase K. *et al.* (2000a) Conditionally immortalized brain capillary endothelial cell lines established from a transgenic mouse harboring temperature-sensitive simian virus 40 large T-antigen gene. *AAPS PharmSci.* **2**, article 27, doi: 10.1208/ps020327.URL http://www.aapspharmsci.org/

Hosoya K., Takashima T., Tetsuka K., Nagura T., Ohtsuki S., Takanaga H., Ueda M., Yanai N., Obinata M. and Terasaki T. (2000b) mRNA expression and transport characterization of conditionally immortalized rat brain capillary endothelial cell lines; a new in vitro BBB model for drug targeting. *J. Drug Target.* **8**, 357–370.

Huber J. D., Witt K. A., Hom S., Egleton R. D., Mark K. S. and Davis T. P. (2001) Inflammatory pain alters blood–brain barrier permeability and tight junctional protein expression. *Am. J. Physiol. Heart Circ. Physiol.* **280**, H1241–H1248.

Iizasa H., Bae S. H., Asashima T., Kitano T., Matsunaga N., Terasaki T., Kang Y. S. and Nakashima E. (2002) Augmented expression of the tight junction protein occludin in brain Endothelial cell line TR-BBB by rat angiopoietin-1 expressed in baculovirus-infected sf plus insect cells. *Pharm. Res.* **19**, 1757–1760.

Janzer R. C. and Raff M. C. (1987) Astrocytes induce blood–brain barrier properties in endothelial cells. *Nature* **325**, 253–257.

Jones N., Master Z., Jones J., Bouchard D., Gunji Y., Sasaki H., Daly R., Alitalo K. and Dumont D. J. (1999) Identification of Tek/Tie2 binding partners. Binding to a multifunctional docking site mediates cell survival and migration. *J. Biol. Chem.* **274**, 30896–30905.

Kalaria R. N., Cohen D. L., Premkumar D. R., Nag S., LaManna J. C. and Lust W. D. (1998) Vascular endothelial growth factor in Alzheimer's disease and experimental cerebral ischemia. *Brain. Res. Mol. Brain Res.* **62**, 101–105.

Knuckey N. W., Finch P., Palm D. E., Primiano M. J., Johanson C. E., Flanders K. C. and Thompson N. L. (1996) Differential neuronal and astrocytic expression of transforming growth factor beta isoforms in rat hippocampus following transient forebrain ischemia. *Brain Res. Mol. Brain Res.* **40**, 1–14.

Lee S. W., Kim W. J., Choi Y. K., Song H. S., Son M. J., Gelman I. H., Kim Y. J. and Kim K. W. (2003) SSeCKS regulates angiogenesis and tight junction formation in blood–brain barrier. *Nat. Med.* **9**, 900–906.

Lesne S., Blanchet S., Docagne F., Liot G., Plawinski L., MacKenzie E. T., Auffray C., Buisson A., Pietu G. and Vivien D. (2002) Transforming growth factor-beta1-modulated cerebral gene expression. *J. Cereb. Blood Flow Metab.* **22**, 1114–1123.

Lindahl P., Johansson B. R., Leveen P. and Betsholtz C. (1997) Pericyte loss and microaneurysm formation in PDGF-B-deficient mice. *Science* **277**, 242–245.

Little D., Dean R. A., Young K. M., McKane S. A., Martin L. D., Jones S. L. and Blikslager A. T. (2003) PI3K signaling is required for prostaglandin-induced mucosal recovery in ischemia-injured porcine ileum. *Am. J. Physiol. Gastrointest. Liver Physiol.* **284**, G46–G56.

Maisonpierre P. C., Suri C., Jones P. F. *et al.* (1997) Angiopoietin-2, a natural antagonist for Tie2 that disrupts in vivo angiogenesis. *Science* **277**, 55–60.

Mandriota S. J., Pyke C., Di Sanza C., Quinodoz P., Pittet B. and Pepper M. S. (2000) Hypoxia-inducible angiopoietin-2 expression is mimicked by iodonium compounds and occurs in the rat brain and skin in response to systemic hypoxia and tissue ischemia. *Am. J. Pathol.* **156**, 2077–2089.

Martin-Padura I., Lostaglio S., Schneemann M. *et al.* (1998) Junctional adhesion molecule, a novel member of the immunoglobulin superfamily that distributes at intercellular junctions and modulates monocyte transmigration. *J. Cell Biol.* **142**, 117–127.

McCarthy K. M., Skare I. B., Stankewich M. C., Furuse M., Tsukita S., Rogers R. A., Lynch R. D. and Schneeberger E. E. (1996) Occludin is a functional component of the tight junction. *J. Cell Sci.* **109**, 2287–2298.

Miller R. H. and Raff M. C. (1984) Fibrous and protoplasmic astrocytes are biochemically and developmentally distinct. *J. Neurosci.* **4**, 585–592.

Mooradian A. D., Haas M. J. and Chehade J. M. (2003) Age-related changes in rat cerebral occludin and zonula occludens-1 (ZO-1). *Mech. Ageing Dev.* **124**, 143–146.

Nishiyama R., Sakaguchi T., Kinugasa T., Gu X., MacDermott R. P., Podolsky D. K. and Reinecker H. C. (2001) Interleukin-2 receptor beta subunit-dependent and -independent regulation of intestinal epithelial tight junctions. *J. Biol. Chem.* **276**, 35571–35580.

Nitta T., Hata M., Gotoh S., Seo Y., Sasaki H., Hashimoto N., Furuse M. and Tsukita S. (2003) Size-selective loosening of the blood–brain barrier in claudin-5-deficient mice. *J. Cell Biol.* **161**, 653–660.

Obinata M. (1997) Conditionally immortalized cell lines with differentiated functions established from temperature-sensitive T-antigen transgenic mice. *Genes Cells* **2**, 235–244.

Ostermann G., Weber K. S., Zernecke A., Schroder A. and Weber C. (2002) JAM-1 is a ligand of the beta (2) integrin LFA-1 involved in transendothelial migration of leukocytes. *Nat. Immunol.* **3**, 151–158.

Pardridge W. M. (1999) Blood–brain barrier biology and methodology. *J. Neurovirol.* **5**, 556–569.

Peters A., Josephson K. and Vincent S. L. (1991) Effects of aging on the neuroglial cells and pericytes within area 17 of the rhesus monkey cerebral cortex. *Anat. Rec.* **229**, 384–398.

Procopio W. N., Pelavin P. I., Lee W. M. and Yeilding N. M. (1999) Angiopoietin-1 and -2 coiled coil domains mediate distinct homo-oligomerization patterns, but fibrinogen-like domains mediate ligand activity. *J. Biol. Chem.* **274**, 30196–30201.

Shimizu S., Eguchi Y., Kamiike W., Itoh Y., Hasegawa J., Yamabe K., Otsuki Y., Matsuda H. and Tsujimoto Y. (1996) Induction of apoptosis as well as necrosis by hypoxia and predominant prevention of apoptosis by Bcl-2 and Bcl-XL. *Cancer Res.* **56**, 2161–2166.

Stelwagen K., McFadden H. A. and Demmer J. (1999) Prolactin, alone or in combination with glucocorticoids, enhances tight junction formation and expression of the tight junction protein occludin in mammary cells. *Mol. Cell. Endocrinol.* **156**, 55–61.

Takahashi R., Hirabayashi M., Yanai N., Obinata M. and Ueda M. (1999) Establishment of SV40-tsA58 transgenic rats as a source of conditionally immortalized cell lines. *Exp. Anim.* **48**, 255–261.

Terasaki T. and Hosoya K. (2001) Conditionally immortalized cell lines as a new in vitro model for the study of barrier functions. *Biol. Pharm. Bull.* **24**, 111–118.

Terasaki T., Ohtsuki S., Hori S., Takanaga H., Nakashima E. and Hosoya K. (2003) New approaches to in vitro models of the blood–brain barrier drug transport. *Drug Discov. Today* **15**, 944–954.

Tetsuka K., Hosoya K., Ohtsuki S., Takanaga H., Yanai N., Ueda M., Obinata M. and Terasaki T. (2001) Acidic amino acid transport characteristics of a newly developed conditionally immortalized rat type 2 astrocyte cell line (TR-AST). *Cell Struct. Funct.* **26**, 197–203.

Valenzuela D. M., Griffiths J. A., Rojas J. *et al.* (1999) Angiopoietins 3 and 4: diverging gene counterparts in mice and humans. *Proc. Natl Acad. Sci. USA* **96**, 1904–1909.

Verbeek M. M., de Waal R. M., Schipper J. J. and Van Nostrand W. E. (1997) Rapid degeneration of cultured human brain pericytes by amyloid beta protein. *J. Neurochem.* **68**, 1135–1141.

Wang W., Dentler W. L. and Borchardt R. T. (2001) VEGF increases BMEC monolayer permeability by affecting occludin expression and tight junction assembly. *Am. J. Physiol. Heart Circ. Physiol.* **280**, H434–H440.

Woo P. L., Ching D., Guan Y. and Firestone G. L. (1999) Requirement for Ras and phosphatidylinositol 3-kinase signaling uncouples the glucocorticoid-induced junctional organization and transepithelial electrical resistance in mammary tumor cells. *J. Biol. Chem.* **274**, 32818–32828.

Zhang Z. G., Zhang L., Croll S. D. and Chopp M. (2002) Angiopoietin-1 reduces cerebral blood vessel leakage and ischemic lesion volume after focal cerebral embolic ischemia in mice. *Neuroscience* **113**, 683–687.

Journal of Neurochemistry, 2004, **90**, 526–536 doi:10.1111/j.1471-4159.2004.02537.x

Functional expression of rat ABCG2 on the luminal side of brain capillaries and its enhancement by astrocyte-derived soluble factor(s)

Satoko Hori,*,†,‡ Sumio Ohtsuki,*,†,‡ Masanori Tachikawa,* Norihisa Kimura,* Tetsu Kondo,* Masahiko Watanabe,‡,§ Emi Nakashima‡,¶ and Tetsuya Terasaki*,†,‡

**Department of Molecular Biopharmacy and Genetics, Graduate School of Pharmaceutical Sciences, Tohoku University, Sendai, Japan*

†New Industry Creation Hatchery Center, Tohoku University, Sendai, Japan

‡CREST and SORST of the Japan Science and Technology Agency (JST), Japan

§Department of Anatomy, Hokkaido University School of Medicine, Sapporo, Japan

¶Department of Pharmaceutics, Kyoritsu College of Pharmacy, Tokyo, Japan

Abstract

The purpose of the present study was to clarify the expression, transport properties and regulation of ATP-binding cassette G2 (ABCG2) transporter at the rat blood–brain barrier (BBB). The rat homologue of ABCG2 (rABCG2) was cloned from rat brain capillary fraction. In rABCG2-transfected HEK293 cells, rABCG2 was detected as a glycoprotein complex bridged by disulfide bonds, possibly a homodimer. The protein transported mitoxantrone and BODIPY-prazosin. In rat brain capillary fraction, rABCG2 protein was also detected as a glycosylated and disulfide-linked complex. Immunohistochemical analysis revealed that rABCG2 was localized mainly on the luminal side of rat brain capillaries, suggesting that rABCG2 is involved in brain-to-blood efflux transport. For the regulation study, conditionally immortalized rat brain capillary endothelial (TR-BBB13), astrocyte (TR-AST4) and pericyte (TR-PCT1) cell lines were used as an *in vitro* BBB model. Following treatment of TR-BBB13 cells with conditioned medium of TR-AST4 cells, the Ko143 (an ABCG2-specific inhibitor)-sensitive transport activity and rABCG2 mRNA level were significantly increased, whereas conditioned medium of TR-PCT1 cells had no effect. These results suggest that rat brain capillaries express functional rABCG2 protein and that the transport activity of the protein is up-regulated by astrocyte-derived soluble factor(s) concomitantly with the induction of rABCG2 mRNA.

Keywords: ABCG2, astrocyte, blood–brain barrier, *in vitro* BBB model.

J. Neurochem. (2004) **90**, 526–536.

ABCG2 (BCRP/MXR/ABCP1), a member of the ATP-binding cassette (ABC) superfamily, was originally isolated from cancer cells resistant to anticancer drugs (Doyle *et al.* 1998). ABCG2 is also expressed in normal tissues, such as small intestine, liver and placenta (Maliepaard *et al.* 2001), and presumed to play a protective role against toxic substances and metabolites.

It has been reported recently that ABCG2 is expressed in isolated porcine brain capillaries (Eisenblatter and Galla 2002; Eisenblatter *et al.* 2003). Moreover, ABCG2 is reported to be localized on the luminal side of human brain capillaries (Cooray *et al.* 2002). Brain capillary endothelial cells (BCECs) constitute the blood–brain

Received February 16, 2004; revised manuscript received April 2, 2004; accepted April 2, 2004.

Address correspondence and reprint requests to Professor Tetsuya Terasaki, Department of Molecular Biopharmacy and Genetics, Graduate School of Pharmaceutical Sciences, Tohoku University, Aoba, Aramaki, Aoba-ku, Sendai 980–8578, Japan.
E-mail: terasaki@mail.pharm.tohoku.ac.jp

Abbreviations used: ABC, ATP-binding cassette; AST, (PCT)-CM, conditioned medium of TR-AST (TR-PCT) cells; BBB, blood–brain barrier; BCEC, brain capillary endothelial cell; P-gp, P-glycoprotein; TR-AST, conditionally immortalized rat astrocyte cell line; TR-BBB, conditionally immortalized rat brain capillary endothelial cell line; TR-PCT, conditionally immortalized rat pericyte cell line.

barrier (BBB), which prevents non-specific entry of compounds into the brain. Therefore, ABCG2 present in BCECs may act to restrict the penetration of xenobiotics into the brain and to pump out potential toxins or metabolites from the brain. ABCG2 transports sulfated conjugates of drugs and sterols (Suzuki *et al.* 2003), whereas P-glycoprotein (P-gp), a well-characterized efflux transporter at the BBB, preferentially transports more hydrophobic compounds. Therefore, it is conceivable that ABCG2 functions as a new efflux transporter at the BBB. However, the brain penetration of a dietary carcinogen, which is known to be a substrate of ABCG2, was not significantly increased, whereas the intestinal uptake and the fetal penetration of ABCG2 substrate drugs were increased in ABCG2 knockout mice (Jonker *et al.* 2002; van Herwaarden *et al.* 2003). The reason for this apparent discrepancy is still unknown.

ABCG2 functions as a homodimer and its transport activity was lost when dimer formation was blocked in cDNA-transfected cells (Kage *et al.* 2002). Single amino acid substitutions of ABCG2 in the transmembrane (TM) domain of ABCG2 alter the substrate specificity (Miwa *et al.* 2003). In normal human tissues, a splicing variant of ABCG2 has been identified in the placenta (Imai *et al.* 2002). It is also possible that ABCG2 dimerizes with other ABCG subtypes, and that the resulting heterodimers transport different substrates compared with those transported by the homodimer *in vivo*, as shown in the case of the *Drosophila* homologue of ABCG1 (Ewart *et al.* 1994). It is therefore important to clarify whether the sequence of ABCG2 is functional and the protein forms a functional dimer at the BBB.

The up-regulation of ABCG2 expression in brain vessels has been detected in brain tumors (Zhang *et al.* 2003). Therefore, the functional expression of ABCG2 at the BBB is presumably inducible. Indeed, our recent studies have shown that the transport activities of taurine transporter and xCT were regulated by external stimuli (Hosoya *et al.* 2002; Kang *et al.* 2002) and that astrocytes and pericytes surrounding brain capillaries induced the expression of tight-junction protein (Hori *et al.* 2004). An understanding of the functional regulation of ABCG2 should throw light on the physiological function of ABCG2 at the BBB.

The purpose of this study was to investigate ABCG2 protein expression and modification, as well as the transport properties using ABCG2-overexpressing cells (transduced with cDNA isolated from rat brain capillary fraction), and a conditionally immortalized rat BCEC cell line in order to clarify the functional expression of ABCG2 at the rat BBB. Furthermore, we investigated the effect of astrocyte- and pericyte-derived factors on ABCG2 function by using conditionally immortalized BBB cell lines of the same maturational stage, strain, and genetic background (Terasaki *et al.* 2003).

Materials and methods

Animals

Male Wistar rats, weighing 150–250 g, were purchased from Charles River (Yokohama, Japan). The investigations using rats described in this report conformed to the guidelines established by the Animal Care Committee, Graduate School of Pharmaceutical Sciences, Tohoku University.

Reagents

Endothelial cell growth factor (ECGF) was purchased from Boehringer Mannheim (Mannheim, Germany); benzylpenicillin potassium and streptomycin sulfate were purchased from Wako Pure Chemical Industries (Osaka, Japan). Ko143 was a generous gift from Dr A Schinkel (Netherlands Cancer Institute, Amsterdam, the Netherlands) (Allen et al. 2002). All other chemicals were commercial products of analytical grade.

Cell cultures

TR-BBB13, TR-AST4 and TR-PCT1 cells are conditionally immortalized BCEC, astrocyte and pericyte cell lines (Hosoya *et al.* 2000b; Tetsuka *et al.* 2001; Asashima *et al.* 2002) that have been used as an *in vitro* BBB model (Terasaki *et al.* 2003). The cells were grown in Dulbecco's modified Eagle's medium (DMEM, Nissui Pharmaceutical, Tokyo, Japan) supplemented with 20 mM sodium bicarbonate, 15 ng/mL ECGF, 100 U/mL benzylpenicillin potassium, 100 μg/mL streptomycin sulfate and 10% fetal bovine serum (Moregate, Bulimba, Australia) (culture-medium A). TR-AST4 cells, TR-PCT1 cells and HEK293 cells (American Type Culture Collection, Rockville, MD, USA) were cultured in culture-medium A without ECGF (culture-medium B). TR-BBB13 cells were seeded onto rat-tail collagen type I-coated tissue culture dishes (BD Biosciences, Franklin Lakes, NJ, USA). The BBB cell lines were maintained at 33°C, which is a permissive temperature at which temperature-sensitive SV40 large T-antigen is activated, in a humidified atmosphere of 95% air and 5% CO_2. HEK293 cells were cultured at 37°C under 5% CO_2/air.

Quantitative real-time PCR analysis

Under deep anesthesia induced with ketamine and xylazine, adult rats were transcardially perfused with phosphate-buffered saline (PBS) to remove blood. Rat tissues were obtained after this perfusion. Total RNA was extracted from rat tissues and TR-BBB13 cells with TRIZOL reagent (Life Technologies, Grand Island, NY, USA) and RNeasy kit (Qiagen, Tokyo, Japan) according to the manufacturer's protocol, respectively. RNA integrity was checked by electrophoresis on an agarose gel. Single-stranded cDNA was prepared from 1 μg total RNA by RT (ReverTraAce, Toyobo, Osaka, Japan) using oligo (dT) primer. Quantitative real-time PCR analysis was performed using an ABI PRISM 7700 sequence detector system (PE Applied Biosystems, Foster City, CA, USA) with 2 X SYBR Green PCR Master Mix (PE Applied Biosystems) as per the manufacturer's protocol. To quantify the amount of specific mRNA in the samples, a standard curve was generated for each run using pGEM-T Easy vector (Promega, Madison, WI, USA) containing ABCG2 or β-actin (dilution ranging from 0.1 fg/μL to 1 ng/μL). This enabled standardization of the initial mRNA content

of TR-BBB13 cells relative to the quantity of β-actin. The control lacking the RT enzyme was assayed in parallel to monitor any possible genomic contamination. The PCR was performed through 40 cycles of 95°C for 30 s, 60°C for 1 min, and 72°C for 1 min after preincubation at 95°C for 10 min using specific primers. The sequences of the primers were as follows: sense primer (S1) 5′-CAATGGGATCATGAAACCTG-3′ and antisense primer (AS1) 5′-GAGGCTGATGAATGGAGAA-3′ for ABCG2 (GenBank accession number NM011920); sense primer 5′-TTTGAGACCTTCAA CACCCC-3′ and antisense primer 5′-ATAGCTCTTCTCCAGG GAGG-3′ for β-actin (GenBank accession number NM031144).

Isolation of rat homologue of ABCG2 (rABCG2) cDNA

Rat brain capillary fraction was collected from brain homogenates as described previously (Hosoya *et al.* 2000b). Briefly, cerebrum excised from rats was dissected into 2-mm pieces, and homogenized using a Potter-Elvehjem homogenizer in PBS. Homogenate was added to the same volume of 32% dextran solution, and then centrifuged (4500 × *g*, 10 min, 4°C). The resulting pellets were washed in PBS to obtain the enriched capillary fraction. Total RNA was extracted from rat brain capillary fraction with TRIZOL reagent according to the manufacturer's protocol. To prepare 5′- or 3′-cDNA fragments, the total RNA was reverse-transcribed by PowerScript™ RT enzyme (BD Biosciences) in the presence of modified oligo (dT) primers, which contain sequences for annealing with Universal Primer Mix (UPM) (BD Biosciences). After generation of the 5′- and 3′-cDNA fragments, 5′- or 3′-RACE PCR was performed using two sets of primers (UPM and 5′RACE 1, or UPM and 3′RACE1, respectively) and Advantage 2 Polymerase (BD Biosciences). The sequences of the primers were as follows: 5′RACE 1 primer 5′-CCCCGTGGGTCTTTCCTTGCTGCTAGG-3′, 3′RACE1 primer 5′-CTGGCCATAGCCGCAGGCCAAAGCG-3′.

To obtain three overlapping PCR products, PCR was performed using three sets of primers (S1 and AS1, S2 and AS2, and S3 and AS3) with Ex Taq (Takara, Shiga, Japan). The sequences of S1 and AS1 primers are given above. The sequences of the other primers were as follows: S2 primer 5′-GGACTCAAGCACAGCAAATGC-3′, AS2 primer 5′-CTCCACAGCTGACACACTG-3′, S3 primer 5′-CCTGACTACCAACCAGTG-3′ and AS3 primer 5′-GCTGTGAAGCCATATCGAGG-3′. All PCR procedures were performed at least twice, and the PCR products were subcloned into a plasmid vector using pGEM-T Easy Vector and amplified in *Escherichia coli*. Several independent clones obtained from each PCR procedure were sequenced from both directions using a DNA sequencer (CEQ2000XL DNA Analysis System; Beckman Coulter, Fullerton, CA, USA).

Construction of plasmid vector and transfectant

rABCG2 cDNA was generated by RT-PCR from total RNA of rat brain capillary fraction with the following primers: sense primer with a BamHI site (underlined), 5′-GGATCCGATGTCTTCTAGT-AATGAC-3′, antisense primer with an XhoI site (underlined), 5′-CTCGAGCAATAGTCCTTTCAAGGG-3′. The PCR product was subcloned into a plasmid vector using the pGEM-T Easy vector for sequencing. The cDNA segment 100% identical with the full-length of rABCG2 was cut from pGEM-T Easy with BamHI and XhoI (Takara), and ligated into pCMV-Tag3A (Stratagene, La Jolla, CA, USA), which contains the c-myc epitope (EQKLISEEDL) from the human c-myc gene in the upstream of the multiple cloning site (pCMV-Tag3A/rABCG2). To obtain rABCG2-overexpressing cells, pCMV-Tag3A/rABCG2 was transfected into HEK293 cells using Lipofectamine plus (Life Technologies) according to the manufacturer's procedure. G418 (800 μg/mL)-resistant cells were picked up, and myc-tagged rABCG2-expressing cells (HEK293/rABCG2myc) were selected by western blot analysis of ABCG2.

Antibody preparation

Polyclonal antibodies to ABCG2 were raised against amino acid residues 1–34 (G2-Ab1) and 305–343 (G2-Ab2) of mouse ABCG2 (GenBank accession number AF140218). The polypeptides were expressed as glutathione *S*-transferase (GST) fusion proteins using pGEX4T-2 plasmid vector (Amersham Biosciences, Uppsala, Sweden). The fusion protein was purified with glutathione-Sepharose 4B (Amesham Biosciences), emulsified with Freund's complete adjuvant (Difco, Detroit, MI, USA), and injected subcutaneously into female Hartley guinea pigs at intervals of two weeks. Two weeks after the sixth injection, affinity-purified antibodies were prepared, first using protein G-Sepharose (Amersham Biosciences) and then using antigen peptides coupled to cyanogen bromide-activated Sepharose 4B (Amersham Biosciences). For the preparation of affinity media, polypeptides devoid of GST were obtained by elution of the cleaved polypeptide after in-column thrombin digestion of fusion proteins bound to glutathione-Sepharose.

Western blot analysis

Rat tissues were obtained after perfusion in the same way as for the quantitative real-time PCR analysis. Rat tissues, HEK293 cells, HEK293/rABCG2myc cells, or TR-BBB13 cells were homogenized in buffer containing 10 mM Tris-HCl (pH 7.4), 10 mM NaCl, 1.5 mM $MgCl_2$, 1 mM phenylmethylsulfonyl fluoride (PMSF), and a protease-inhibitor cocktail (Sigma Chemical Co., St. Louis, MO, USA). The homogenized samples were centrifuged at 10 000 × *g* for 10 min and the supernatants were collected. These supernatants were centrifuged at 100 000 × *g* for 30 min, and a crude membrane fraction was obtained from the pellets. The pellets were suspended in buffer containing 10 mM Tris-HCl (pH 7.4), 1 mM EDTA, 150 mM NaCl, 4% CHAPS, 1 mM PMSF, and a protease-inhibitor cocktail. The protein concentration of the lysates was measured by the Bradford method using Bio-Rad Protein Assay reagent (Bio-Rad, Hercules, CA, USA). Deglycosylation was carried out by incubating the crude membrane protein fraction with *N*-glycosidase F (Boehringer Mannheim) for 30 min at 37°C. Protein samples (tissues, 20 μg; TR-BBB13 cells, 80 μg per lane) were resolved by 7.5% SDS–polyacrylamide gel (Bio-Rad) electrophoresis and subsequently electrotransferred to nitrocellulose membranes. Membranes were treated with blocking buffer (4% skimmed milk in 25 mM Tris-HCl (pH 8.0), 125 mM NaCl, 0.1% Tween 20) for 2 h at room temperature and incubated with anti-ABCG2 antibodies (G2-Ab1, 1 μg/mL for HEK293/rABCG2myc cells, rat tissues and TR-BBB13 cells; G2-Ab2, 0.5 μg/mL for HEK293/rABCG2myc cells) or anti-c-myc antibody (0.1 μg/mL; Bethyl Laboratories, Montgomery, TX, USA) as the primary antibody at 4°C for 16 h after blocking. The membranes were washed three times with blocking buffer and incubated with horseradish peroxidase-conju-

gated second antibody. The bands were visualized with an enhanced chemiluminescence kit (SuperSignal; Pierce, Rockford, IL, USA).

Immunohistochemical analysis in HEK293/rABCG2myc cells and rat brain

HEK293 cells or HEK293/rABCG2myc cells were seeded at a density of 5×10^4 cells on chamber slides (4.0 cm^2; Asahi Techno Glass Corp., Tokyo, Japan), and cultured overnight. The following procedures were carried out at room temperature. Cells were washed with PBS and fixed with 4% paraformaldehyde in PBS for 20 min. Cells were incubated with 0.1% Triton X-100 in PBS for 30 min and then incubated with 10% goat serum for 30 min. After further washing with PBS, the cells were incubated with anti-c-myc antibody (1 μg/mL; Santa Cruz Biotechnology, Santa Cruz, CA, USA) as a primary antibody in the presence of 0.1% bovine serum albumin in PBS for 1 h. Cells were then washed with PBS and incubated for 1 h with fluorescein isothiocyanate (FITC)-conjugated second antibody for 1 h. Cells were washed with PBS and immunofluorescence was viewed using a confocal laser scanning microscope (TCS SP, Leica Microsystems, Wetzlar, Germany).

Under deep pentobarbital anesthesia (100 mg/kg of body weight), brains of adult Wistar rats were perfused transcardially with 4% paraformaldehyde in 0.1 M sodium phosphate buffer (PB), pH 7.4, embedded in paraffin wax after dehydration using graded alcohols, and processed for the preparation of paraffin sections (5 μm) with a sliding microtome (SM2000R; Leica Microsystems). Prior to immunohistochemical investigation, paraffin sections were digested with pepsin (1 mg/mL in 0.2 M HCl, Dako, Carpinteria, CA, USA) for 5 min at 37°C to retrieve antigens. For immunofluorescence, sections were incubated at room temperature with 10% normal goat serum for 30 min, guinea pig anti-ABCG2 antibody (G2-Ab2) 2 μg/mL singly or in combination with rabbit glucose transporter 1 (GLUT1) antibody (1 : 5000; Chemicon, Temecula, CA, USA) overnight, FITC- or rhodamine-conjugated secondary antibody for 2 h. Some sections were counterstained with 3 μg/mL propidium iodide for 5 min. Photographs were taken with a confocal laser scanning microscope (TCS SP, Leica Microsystems).

Transport assay

For transport studies, HEK293 cells or HEK293/rABCG2myc cells were incubated for 30 min at 37°C in a medium, with or without 10 μM Ko143, a specific ABCG2 inhibitor. After the 30-min preincubation period, the cells were washed with ice-cold medium, resuspended in a medium containing 20 μM mitoxantrone, with or without 10 μM Ko143, and incubated for a further 1 h at 37°C. The cells were then washed with ice-cold PBS and placed on ice until required for measurement. For efflux studies, the cells were incubated for 60 min at 37°C with BODIPY-prazosin (250 nM) (Molecular Probes, Eugene, OR, USA) and then allowed to efflux for 30 min in a medium, with or without 10 μM Ko143. The cells were then washed with ice-cold PBS and placed on ice until required for measurement. Relative cellular accumulation of BODIPY-prazosin and mitoxantrone was determined by flow cytometry with a 488 nm argon laser/530 nm bandpass filter and a 635 nm red diode laser/661 nm bandpass filter, respectively (FACs Calibur; BD Biosciences). At least 20 000 events were collected. Debris was eliminated by gating on forward versus side scatter. The mean channel number for each histogram was used as a measure of drug fluorescence for the calculation.

Effects of conditioned medium of TR-AST4 cells (AST-CM) and TR-PCT1 cells (PCT-CM) on the drug transport activity in TR-BBB13 cells

AST-CM and PCT-CM were obtained as described previously (Hori *et al.* 2004). TR-BBB13 cells were seeded at a density of 1×10^5 cells/well on rat-tail collagen I-coated 24-well plates (BD Biosciences) and cultured for 24 h at 33°C. TR-BBB13 cells were treated with AST-CM or PCT-CM for 24 h at 33°C. After removal of the culture medium, the cells were washed with extracellular fluid (ECF) buffer (122 mM NaCl, 25 mM $NaHCO_3$, 3 mM KCl, 1.4 mM $CaCl_2$, 2 mM $MgSO_4$, 0.4 mM K_2HPO_4, 10 mM D-glucose, 10 mM HEPES (pH 7.4), 290 ± 15 mOsm/kg). The transport study was performed at 37°C, the physiological temperature. The cells were pretreated at 37°C for 30 min in the presence or the absence of 0.5 μM Ko143, then uptake was initiated by adding ECF buffer containing 20 μM mitoxantrone or 250 nM BODIPY-prazosin, with or without Ko143, and incubation was continued for a further 1 h at 37°C. The efflux transport activity was terminated by removing the solution and immersing the cells in ice-cold ECF buffer. The cells were collected and placed on ice until required for measurement. Flow cytometry analysis was performed as described above.

Data analysis

Unless otherwise indicated, all data represent the mean ± SEM. An unpaired, two-tailed Student's *t*-test was used to determine the significance of differences between two groups means. One-way ANOVA followed by the modified Fisher's least-squares difference method was used to assess the statistical significance of differences among means of more than two groups.

Results

mRNA expression of ABCG2 in rat brain capillary fraction and tissues

Quantitative real-time PCR analysis was performed to determine the ABCG2 mRNA levels in rat brain capillary fraction, small intestine, kidney, heart and brain (Fig. 1a). High mRNA expression of ABCG2 was detected in rat brain capillary fraction. When each mRNA level was indicated as a relative ratio to that in rat small intestine, the ABCG2 mRNA levels in rat kidney, heart, brain and brain capillary fraction were 1.16 ± 0.17, 0.23 ± 0.02, 0.19 ± 0.03 and 6.59 ± 0.46, respectively. Moreover, the ABCG2 mRNA level in the rat brain capillary fraction was enriched by 34.7-fold compared with that in rat brain.

cDNA cloning of rat homologue of ABCG2 (rABCG2) from rat brain capillary fraction

rABCG2 cDNA was isolated from the rat brain capillary fraction. The cDNA sequence (GenBank accession number AB105817) has a single open reading frame (1974 bp),

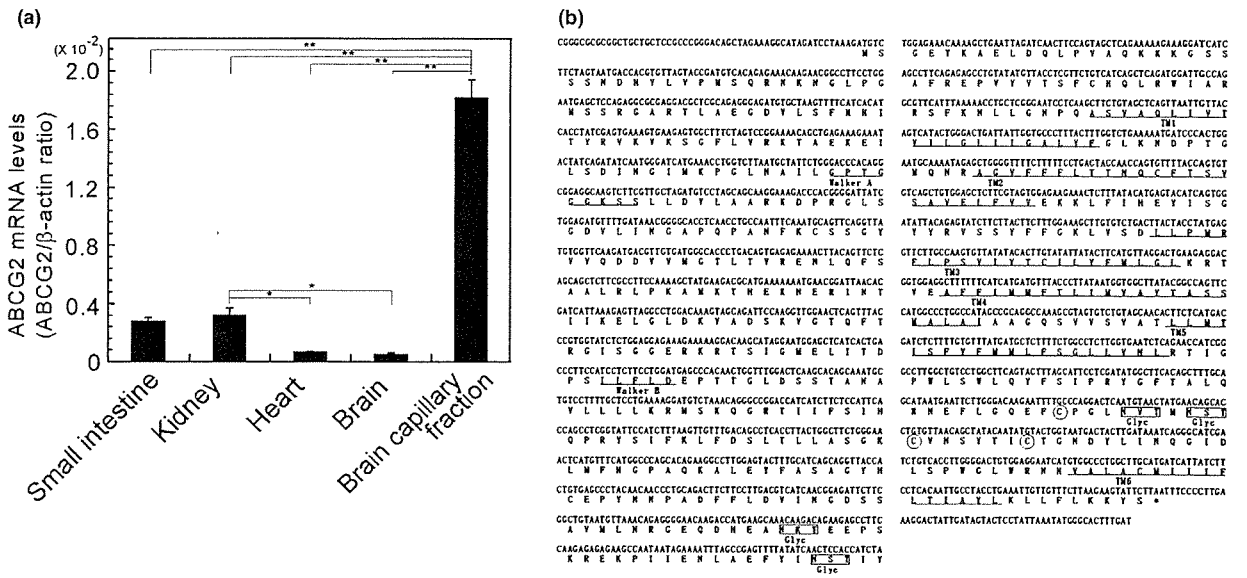

Fig. 1 rABCG2 cDNA cloning from rat brain capillary fraction. (a) The ABCG2 mRNA levels in rat brain capillary fraction and other tissues were determined by quantitative real-time PCR analysis. Each column represents the mean SEM ($n = 3$). $^{**}p < 0.01$, $^{*}p < 0.05$, significant difference. (b) Nucleotide sequence and deduced amino acid sequence of rABCG2 cDNA. The deduced amino acid sequence is shown below the nucleotide sequence. The Walker A and B motifs, and six putative transmembrane domains (TM1-6) are underlined. Open circles indicate potential sites for disulfide bonds. Glyc, potential N-glycosylation sites; GenBank accession number AB105817.

which corresponds to 657 amino acid residues (Fig. 1b). Its deduced amino acid sequence is 81.2, 93.0 and 80.7% identical with human, mouse and porcine ABCG2, respectively. Further amino acid analysis revealed that the ATP-binding domain is located at position 54–268. This domain includes the Walker A and B motifs at 79–86 (GPTGGGKS) and 205–209 (ILFLD), respectively. This N-terminal region includes six putative TM domains (TM1-6) (Fig. 1b). Four potential sites for N-linked glycosylation are shown in Fig. 1(b). Two N-linked glycosylation sites are located in the loop between TM5 and TM6 at amino acid positions 596–699 (NVT) and 600–602 (NST), and are probably extracellular. The other N-linked glycosylation sites are located at amino acid positions 316–319 (NKT) and 338–340 (NST), which is likely to be in the intracellular part of the protein. Three potential sites for disulfide bonds are located in the loop between TM5 and TM6 at amino acid positions 592 (C), 603 (C) and 610 (C). The sequence of the open reading frame of rABCG2 cDNA in TR-BBB13 cells showed 100% homology with that in rat brain capillary fraction.

Expression and plasma membrane localization of myc-tagged rABCG2 protein in HEK293 cells

The expression of myc-tagged rABCG2 was determined by western blot analysis using anti-c-myc and anti-ABCG2 antibodies (G2-Ab1 and G2-Ab2) (Fig. 2a,b). At the same time, the specificity of G2-Ab1 and G2-Ab2 against rABCG2 was evaluated. In the presence of a reducing agent (2-mercaptoethanol), a single band at ~85 kDa was detected in HEK293/rABCG2myc cells with anti-c-myc antibody, whereas no band was detected in parental HEK293 cells (Fig. 2a). The ~85-kDa protein was also detected with G2-Ab1 and G2-Ab2 (Fig. 2a). In the absence of the reducing agent, bands at ~85 kDa and ~170 kDa were detected in HEK293/rABCG2myc cells with anti-c-myc antibody, G2-Ab1 and G2-Ab2 (Fig. 2b).

Figure 2(c) shows the confocal microscopic images of HEK293/rABCG2myc cells stained with anti-c-myc antibody. Intense immunoactivities at the plasma membrane were detected in HEK293/rABCG2myc cells treated with anti-c-myc antibody, whereas no signals were seen in HEK293/rABCG2myc cells treated with normal mouse immunoglobulin and in the parental cells (HEK293 cells) treated with anti-c-myc antibody (data not shown).

Mitoxantrone and BODIPY-prazosin efflux mediated by rABCG2

The mitoxantrone level in HEK293/rABCG2myc cells was significantly reduced compared with that in HEK 293 cells (the parental cells) (Fig. 3a). Figure 3(a) also shows the effects of various concentrations of Ko143, a specific inhibitor of mouse and human ABCG2, on mitoxantrone accumulation in HEK293/rABCG2myc cells, as measured by

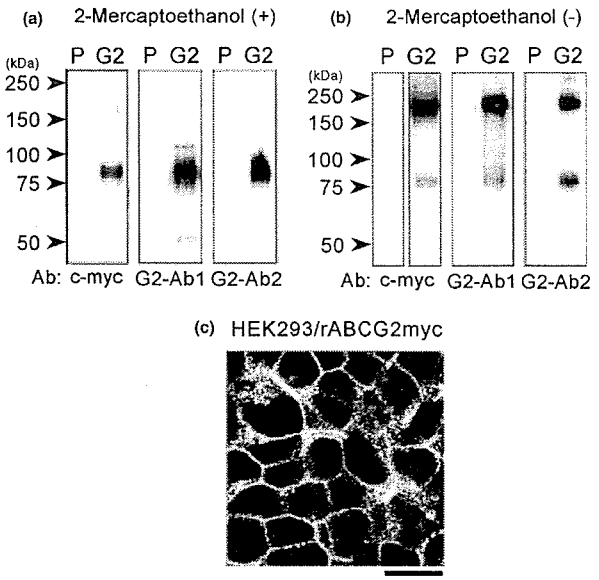

Fig. 2 Expression and localization of myc-tagged rABCG2 in transfected HEK293 cells. (a,b) Western blot analysis using anti-c-myc or anti-ABCG2 (G2-Ab1 and G2-Ab2) antibodies (Ab) against HEK293 cells (P) and HEK293/rABCG2myc cells (G2) in the presence (a) or absence (b) of 2-mercaptoethanol. (c) Immunostaining of myc-tagged rABCG2 in HEK293/rABCG2myc cells. Anti-c-myc antibody was used for immunostaining. Scale bar, 20 μm.

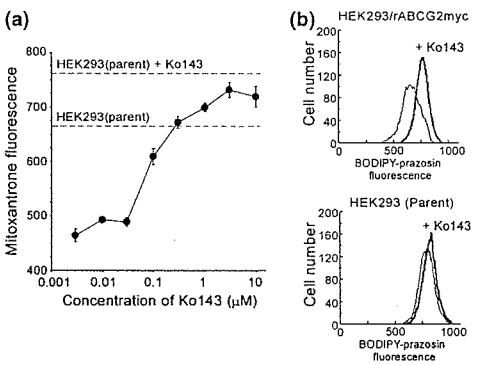

Fig. 3 Functional analysis of rABCG2 in rABCG2-overexpressing cells. (a) Concentration-dependent effect of Ko143 treatment on the intercellular accumulation of mitoxantrone in HEK293/rABCG2myc cells. Horizontal dashed lines show levels of mitoxantrone fluorescence in the parental HEK293 cells in the presence or absence of 10 μM Ko143. Mitoxantrone fluorescence in arbitrary units was determined by flow cytometry with a 635/661 nm filter. Each point represents the mean ± SEM ($n = 4$). (b) Effect of Ko143 (10 μM) on the BODIPY-prazosin (250 nM) efflux in parental HEK293 cells and HEK293/rABCG2myc cells. BODIPY-prazosin fluorescence is in arbitrary units, determined by flow cytometry with a 488/530 nm filter.

flow cytometry. In HEK293/rABCG2myc cells, mitoxantrone levels were elevated by Ko143 treatment in a concentration-dependent manner at concentrations over 0.01 μM, reaching a plateau at 3 μM. In contrast, Ko143 had only a small effect on mitoxantrone levels in the parental HEK293 cells. Based on the midpoint of the cellular accumulation curve in Fig. 3(a), the concentration of Ko143 was approximately 0.1 μM. This value was very close to that in cells overexpressing human ABCG2 (IGROV1/T8 cells) and mouse ABCG2 (MEF3.8/T6400 cells) (Allen *et al.* 2002), suggesting that the inhibitory effect of Ko143 on the ABCG2-mediated transport is essentially the same in rats, humans and mice.

The effect of Ko143 (10 μM) treatment on BODIPY-prazosin efflux is shown in the histograms of Fig. 3(b). In HEK293/rABCG2myc cells, BODIPY-prazosin efflux was inhibited by Ko143 treatment. In contrast, Ko143 had only a small effect on BODIPY-prazosin efflux in the parental HEK293 cells.

Expression and N-linked glycosylation of rABCG2 protein in rat brain capillary fraction and other rat tissues

As rABCG2 has potential N-linked glycosylation sites (Fig. 1b), western blot analysis of rABCG2 was performed with or without *N*-glycosidase F using a crude membrane fraction of rat brain capillary fraction and tissues (Fig. 4a). In the absence of *N*-glycosidase F, bands were detected at

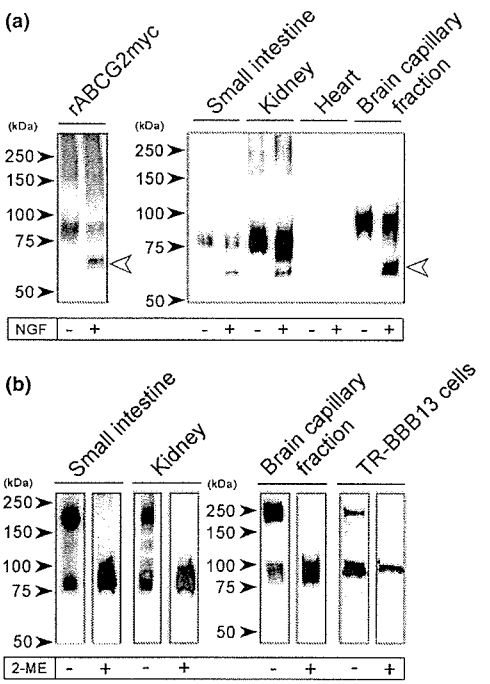

Fig. 4 Western blot analysis of rABCG2 in rat brain capillary fraction, TR-BBB13 cells and other tissues. (a) Protein samples were incubated in the presence (+) or absence (–) of *N*-glycosidase F (NGF). Open arrowheads indicate the expected size of rABCG2. rABCG2myc, HEK293/rABCG2myc cells. (b) Protein samples were incubated in the presence (+) or absence (–) of 2-mercaptoethanol (2-ME).

~85 kDa in rat small intestine and kidney, and at ~100 kDa in rat brain capillary fraction, while no bands were detected in rat heart. Following treatment with *N*-glycosidase F, part of the bands corresponding to rABCG2 shifted to 62 kDa in the apparent molecular mass of bands in rat small intestine, kidney and brain capillary fraction. The 62-kDa band was also detected in HEK293/rABCG2myc cells treated with *N*-glycosidase F.

Disulfide complex of rABCG2 protein in rat brain capillary fraction, TR-BBB13 cells and other rat tissues

Western blot analysis was performed on rat small intestine, kidney, brain capillary fraction and TR-BBB13 cells with or without 2-mercaptoethanol, a reducing agent, in order to clarify whether rABCG2 forms a complex via disulfide bonds (Fig. 4b). In rat small intestine and kidney, single bands at ~85 kDa were detected under reducing conditions. A high-molecular band at ~170 kDa, in addition to the band at ~85 kDa, was also detected under non-reducing conditions. In rat brain capillary fraction, high-molecular bands at ~200 kDa, and ~100 kDa, were detected under non-reducing conditions. In TR-BBB13 cells, two bands were detected at the same position as that of the disulfide-linked complex in rat brain capillary fraction.

Immunostaining of rABCG2 in the cerebral cortex of rat brain

The localization of rABCG2 was determined in the cerebral cortex of adult rats. rABCG2 immunoreactivities were strongly detected in brain capillaries, which are ramified in all cortical layers (Fig. 5a). Immunostaining was observed along the surface of capillaries (Fig. 5b), and was localized to the inner side of capillary endothelium nuclei (Fig. 5b,c, arrowheads). Double immunostaining with GLUT1 (Fig. 5e,f, red), which is known to be expressed in both the luminal and abluminal membrane of brain capillaries (Dobrogowska and Vorbrodt 1999), showed that rABCG2 (Fig. 5d,f, green) overlapped on the luminal membrane of capillaries (arrowheads), but was below the detection threshold on the abluminal membrane (arrows). Such characteristic immunostaining was not seen following the use of preimmune guinea pig immunoglobulin (data not shown). These features indicate that rABCG2 is preferentially expressed on the luminal membrane of rat brain capillaries.

Enhancement of rABCG2-mediated transport in TR-BBB13 cells following treatment with AST-CM

The mitoxantrone and BODIPY-prazosin levels in TR-BBB13 cells reached a steady state after 45 min (data not shown). Ko143 treatment increased the mitoxantrone and BODIPY-prazosin levels in TR-BBB13 cells at 60 min (Fig. 6a,b, control). As Ko143 is a selective inhibitor of ABCG2, as shown by the fact that 0.5 μM Ko143 had little effect on P-gp or MRP1-5 (Allen *et al.* 2002), the Ko143-dependent enhancement of drug transport activity should reflect the inhibition of ABCG2-mediated drug efflux.

The mitoxantrone and BODIPY-prazosin levels were reduced in TR-BBB13 cells at 60 min by treatment with one- to five-fold concentrated AST-CM (Fig. 6a,b). In contrast, PCT-CM did not affect the level of either drug (Fig. 6a,b). Ko143 treatment reversed the fall in the levels of both drugs (Fig. 6a,b, open columns). Moreover, the Ko143-sensitive transport activity of BODIPY-prazosin was significantly increased by treatment with one- to five-fold concentrated AST-CM compared with non-treated cells, and that of mitoxantrone also showed a tendency to increase (Fig. 6c).

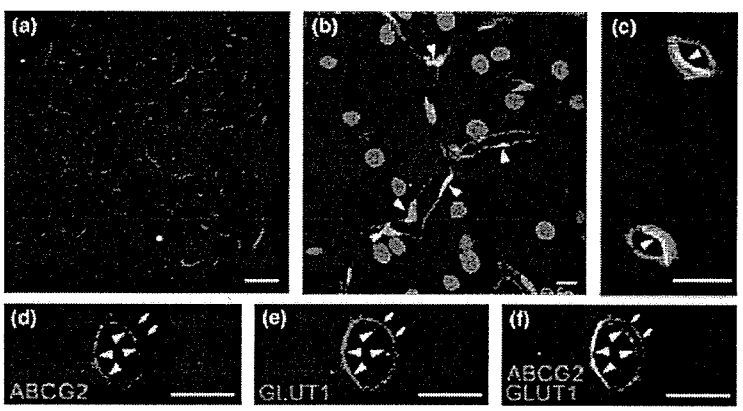

Fig. 5 Immunostaining of rABCG2 in the cerebral cortex of rat brain. (a–c) Low (a) and high (b,c) magnification views of rABCG2 immunostaining in the cerebral cortex. Nuclei were stained by propidium iodide (red; b, c). rABCG2 immunoreactivities (green) were detected in the inner side of capillary endothelium nuclei (arrowheads; b, c). (d–f) Double immunostaining of rABCG2 (green; d, f) and GLUT1 (red; e, f). rABCG2 immunoreactivities were detected on the luminal membrane of capillaries (arrowheads), but not on the abluminal membrane (arrows). Scale bars; (a) 100 μm, (b–f) 10 μm.

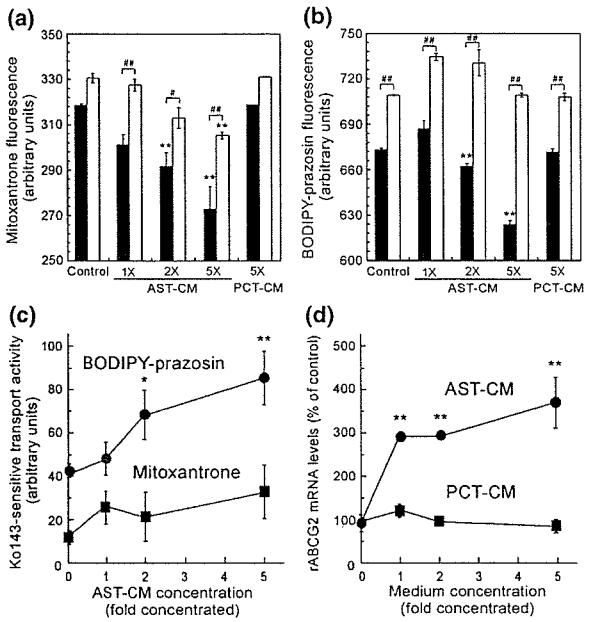

Fig. 6 Functional enhancement of rABCG2 in TR-BBB13 cells produced by treatment with conditioned medium of TR-AST4 cells. (a,b) Effects of one-, two- and five-fold concentrated AST-CM and fivefold concentrated PCT-CM treatment on mitoxantrone (a) and BODIPY-prazosin (b) fluorescence in TR-BBB13 cells in the absence (black columns) or presence (open columns) of 0.5 μM Ko143. Mitoxantrone and BODIPY-prazosin fluorescence in arbitrary units were determined by flow cytometry with a 635/661 nm filter and a 488/530 nm filter, respectively. Each column represents the mean ± SEM ($n = 3$). $^{**}p < 0.01$, significantly different from the respective control. $^{\#\#}p < 0.01$, $^{\#}p < 0.05$, significant difference. (c) The Ko143-sensitive mitoxantrone (■) and BODIPY-prazosin (●) levels in TR-BBB13 cells following treatment with one-, two- and five-fold concentrated AST-CM. The mitoxantrone and BODIPY-prazosin levels are in arbitrary units. Each point represents the mean ± SEM ($n = 3$). $^{**}p < 0.01$, $^{*}p < 0.05$, significantly different from the control. (d) Effects of AST-CM (●) and PCT-CM (■) on the rABCG2 mRNA levels in TR-BBB13 cells for 24 h. The rABCG2 mRNA levels were determined by quantitative real-time PCR analysis. Each point represents the mean ± SEM ($n = 3$). $^{**}p < 0.01$, significantly different from the control.

Induction of rABCG2 mRNA in TR-BBB13 cells following treatment with AST-CM

To determine the effects of astrocytes and pericytes on the mRNA expression of rABCG2, TR-BBB13 cells were cultured with AST-CM or PCT-CM (Fig. 6d). After treatment with one-, two- and five-fold concentrated AST-CM, the rABCG2 mRNA levels were 2.92-, 6.26- and 6.50-fold greater than those in non-treated cells, respectively. The mRNA level of mdr1a, which encodes P-gp and is another ABC transporter at the BBB, was 4.82-fold greater than that in non-treated cells following treatment with five-fold concentrated AST-CM. In contrast, treatment with PCT-CM had no significant effect on the level of either mRNA.

Discussion

The present study provides the first evidence that rABCG2 is mainly localized on the luminal side of rat brain capillaries as a functional transporter that forms a disulfide-linked glycoprotein, possibly a homodimer. Furthermore, the rABCG2-mediated transport activity and the rABCG2 mRNA level were increased in BCECs by soluble factor(s) secreted from astrocytes.

The ABCG2 mRNA and protein in the brain capillary fraction were enriched compared with that in rat brain (Figs 1 and 4), suggesting that ABCG2 is predominantly expressed in rat BCECs. Immunohistochemical analysis confirmed that rABCG2 protein is mainly localized at the luminal membrane of brain capillaries in the rat cortex, whereas it was not detected in other brain cells, such as astrocytes and neurons (Fig. 5). As for pericytes, which surround brain capillaries, the expression of rABCG2 remains unclear without more detailed analysis using electromicroscopy. It has been reported that ABCG2 immunoreactivity was detected in venous and capillary endothelial cells in human peripheral tissues, such as stomach, prostate and ovary, following immunohistochemical analysis (Maliepaard *et al.* 2001), although the function of ABCG2 in these endothelial cells remains obscure.

Although the present study revealed that ABCG2 was localized at the rat BBB, it has been reported that the brain penetration of an ABCG2 substrate was not enhanced in ABCG2 knockout mice (van Herwaarden *et al.* 2003). There could be several explanations for this apparent difference: rABCG2 at the BBB may have a distinct substrate specificity or may not be functional due to species or tissue differences in the sequence and/or the dimer formation of ABCG2. The sequence of rABCG2 was therefore determined using cDNA cloned from rat brain capillary fraction. The clone showed high homology with its human and mouse counterparts. One ABC domain and six TM domains were conserved (Fig. 1b). Furthermore, the amino acids, Q141, E446, R482, N557 and H630, which have been reported to be important for substrate recognition, were conserved (Imai *et al.* 2002; Miwa *et al.* 2003). Mitoxantrone and BODIPY-prazosin were extruded from HEK293/rABCG2myc cells (Fig. 3). Tests show that the substrate specificity is similar to that of mouse and human transporters. These findings suggest that the sequence of rABCG2 is functional at the BBB.

Rat brain capillary fraction, small intestine and kidney highly expressed rABCG2 proteins (Fig. 4), and the tissue distribution of rABCG2 protein is consistent with that of rABCG2 mRNA (Fig. 1a). This is the first report to describe the tissue distribution of rABCG2 at the protein level. Among the tissues tested, rABCG2 in brain capillary fraction is present in the most highly glycosylated form. N-Glycosylation did not alter the level or the pattern of drug resistance mediated by P-gp in transfected cells, although it

contributes to the proper routing or stability of P-gp (Schinkel *et al.* 1993). N-Glycosylation of ABCG2 at the BBB may increase the stability of ABCG2 as far as its membrane localization is concerned.

Although it has been reported that exogenous human ABCG2 forms a homodimer bridged by disulfide bonds in cultured cells (Kage *et al.* 2002), it is still unclear whether ABCG2 functions as a dimer *in vivo*. rABCG2 glycoproteins were detected at the deduced dimeric sizes in rat brain capillary fraction, TR-BBB13 cells, small intestine and kidney under non-reducing conditions (Fig. 4b). The functional expression of rABCG2 in HEK293/rABCG2myc cells indicates that no additional counterpart protein is required for the activity of rABCG2 (Fig. 3), presumably working as a homodimer. Both TR-BBB13 cells and HEK293/rABCG2myc cells exhibited mitoxantrone efflux transport via rABCG2 (Figs 3 and 6). Mitoxantrone resistance was attenuated by inhibiting the homodimer formation of human ABCG2 (Kage *et al.* 2002). These findings strongly suggest that rABCG2 is expressed, at least, as a homodimer bridged by disulfide bonds in rat BCECs.

rABCG2 glycoproteins were detected at the monomeric size as well as the dimeric size in rat brain capillary fraction, TR-BBB13 cells, small intestine and kidney under non-reducing conditions (Fig. 4b). The bands at the monomer size are likely to indicate the premature form of rABCG2 proteins before dimerization, or the existence of non-disulfide-linked rABCG2 proteins. The *Drosophila* homologue of ABCG1 has been reported to have two counterparts, allowing for the transport of different substrates (Ewart *et al.* 1994). TR-BBB13 cells express ABCG1 in addition to ABCG2 (unpublished data). Therefore, dimer formation with ABCG1 may alter the substrate specificity of ABCG2 in rat BCECs.

The efflux transport system at the BBB is important for brain homeostasis and external stimuli may regulate the system. Following treatment with AST-CM, the accumulation of mitoxantrone and BODIPY-prazosin was reduced (Fig. 6a,b). The Ko143-sensitive transport activity of both drugs showed a tendency to increase (Fig. 6c). This result suggests that soluble factors secreted from astrocytes induce ABCG2-mediated transport activity at the BBB. AST-CM increased the rABCG2 mRNA level as well as the Ko143-sensitive transport activity in TR-BBB13 cells (Fig. 6d). In contrast, PCT-CM did not affect either the drug transport activity or the rABCG2 mRNA level. This result suggests that astrocytes under physiological conditions play an important role in regulating ABCG2 function at the BBB, whereas the contribution of pericytes is minor. It has been reported that the expression level of ABCG2 in brain vessels was elevated in glioblastoma (Zhang *et al.* 2003). Glioma cell-derived factors may be involved in the enhancement of the ABCG2 expression as well as normal astrocyte-derived factors.

The Ko143-sensitive transport activity of BODIPY-prazosin continuously increased from one- to five-fold concentrated AST-CM, while the rABCG2 mRNA levels were increased by one-fold concentrated AST-CM and were not significantly increased by higher concentrations (Fig. 6c,d). Therefore, it is possible that both transcriptional regulation and post-translational regulation of rABCG2 function are involved in the functional enhancement of rABCG2. It has been reported that the membrane translocation of ABCG2 was enhanced in hematopoietic stem cells by activating Akt, a serine/threonine kinase (Mogi *et al.* 2003). Our recent investigation has revealed that basic fibroblast growth factor (bFGF), which is known to be an Akt activator, was internalized in BCECs via heparin sulfate proteoglycan expressed on the brain side of the BBB (Deguchi *et al.* 2002). Studies of ABCG2 regulators in AST-CM, including an assessment of how bFGF contributes to this phenomenon, and the difference in the regulators between normal astrocytes and glioma cells should increase our understanding of paracrine interactions between astrocytes and BCECs.

The accumulation of mitoxantrone and BODIPY-prazosin in the presence of Ko143 was also reduced by treatment with AST-CM (Fig. 6a,b), suggesting that AST-CM enhanced the mitoxantrone efflux via mechanisms other than rABCG2 in TR-BBB13 cells. AST-CM increased the level of mdr1a mRNA, encoding P-gp, which transports these drugs as well as ABCG2. Therefore, these findings suggest that the trend of an increase in the rABCG2-unrelated efflux can be partly explained by the up-regulation of P-gp.

The present study strongly suggests that rABCG2 is highly expressed as a functional dimer on the luminal side of brain capillaries. Therefore, it is conceivable that rABCG2 limits the brain penetration of its drug substrates by excreting them to the circulating blood. Indeed, the brain concentration of prazosin after intravenous administration was significantly lower than in other tissues (Dynon *et al.* 1983). It has also been reported that the brain distribution of mitoxantrone is low (Stewart *et al.* 1986). Some hydrophilic compounds present in the brain, such as neurotransmitter metabolites and potential toxins, are excreted from the brain to the circulating blood (Asaba *et al.* 2000; Hosoya *et al.* 2000a; Ohtsuki *et al.* 2002; Mori *et al.* 2003). Among these, dehydroepiandrosterone sulfate (DHEAS) and estrone-3-sulfate are substrates of ABCG2 (Suzuki *et al.* 2003). DHEAS was extruded from a conditionally immortalized mouse BCEC cell line in an ATP-dependent manner (Asaba *et al.* 2000). Taking these findings into consideration, the presence of ABCG2 on the luminal side of the BBB would partly explain the brain-to-blood efflux transport of these endogenous compounds.

It has been reported that coadministration of mitoxantrone and GF120918, which is an inhibitor of ABCG2 and P-gp, did not increase the brain penetration of mitoxantrone (Allen and Schinkel 2002). The present study strongly suggests that

rat BBB expresses ABCG2 which can transport mitoxantrone. Moreover, the rABCG2 expression level in brain capillaries appears to be sufficient for its function to be exhibited, because the intensity of the bands in brain capillary fraction (20 μg/lane) was much greater than that in TR-BBB13 cells (80 μg/lane), which express functional rABCG2 (Fig. 4b). Taken together, these results suggest that rABCG2 is active as an efflux transporter, although other transporter(s) can also exhibit such a function for mitoxantrone. Prazosin is also transported by P-gp (Robey *et al.* 2001), and DHEAS is also transported by MRP4, which has been reported to be expressed in brain capillaries (Zhang *et al.* 2000; Zelcer *et al.* 2003). Further study is needed to elucidate the contribution of ABCG2 to the efflux transport of these compounds across the BBB. Identifying drugs and endogenous compounds that are mainly transported by ABCG2 in the brain is a key issue for clarifying the physiological and pharmacological importance of ABCG2.

In conclusion, the present study demonstrates that rat brain capillaries express functional ABCG2 protein and the transport activity is up-regulated by astrocyte-derived soluble factors. The new finding, that functional ABCG2 is expressed at the rat BBB, contributes to our understanding of the physiological role of ABCG2, and suggests that the influence of ABCG2 as a partner of P-gp cannot be neglected in the development of CNS-acting drugs.

Acknowledgements

The authors wish to thank Dr A. Schinkel (Netherlands Cancer Institute, Amsterdam, the Netherlands) for kindly supplying the ABCG2 inhibitor, Ko143. We would also like to thank Ms. N. Funayama for secretarial assistance. This study was supported, in part, by a Grant-in-Aid for Scientific Research, and a 21st Century Center of Excellence (COE) Program from Japan Society for the Promotion of Science. It was also supported in part by the Industrial Technology Research Grant Program from the New Energy and the Industrial Technology Development Organization (NEDO) of Japan.

References

Allen J. D. and Schinkel A. H. (2002) Multidrug resistance and pharmacological protection mediated by the breast cancer resistance protein (BCRP/ABCG2). *Mol. Cancer Ther.* **1**, 427–434.

Allen J. D., van Loevezijn A., Lakhai J. M., van der Valk M., van Tellingen O., Reid G., Schellens J. H., Koomen G. J. and Schinkel A. H. (2002) Potent and specific inhibition of the breast cancer resistance protein multidrug transporter *in vitro* and in mouse intestine by a novel analogue of fumitremorgin C. *Mol. Cancer Ther.* **1**, 417–425.

Asaba H., Hosoya K., Takanaga H., Ohtsuki S., Tamura E., Takizawa T. and Terasaki T. (2000) Blood–brain barrier is involved in the efflux transport of a neuroactive steroid, dehydroepiandrosterone sulfate, via organic anion transporting polypeptide 2. *J. Neurochem.* **75**, 1907–1916.

Asashima T., Iizasa H., Terasaki T., Hosoya K., Tetsuka K., Ueda M., Obinata M. and Nakashima E. (2002) Newly developed rat brain pericyte cell line, TR-PCT1, responds to transforming growth factor-beta1 and beta-glycerophosphate. *Eur. J. Cell Biol.* **81**, 145–152.

Cooray H. C., Blackmore C. G., Maskell L. and Barrand M. A. (2002) Localisation of breast cancer resistance protein in microvessel endothelium of human brain. *Neuroreport* **13**, 2059–2063.

Deguchi Y., Okutsu H., Okura T., Yamada S., Kimura R., Yuge T., Furukawa A., Morimoto K., Tachikawa M., Ohtsuki S. *et al.* (2002) Internalization of basic fibroblast growth factor at the mouse blood–brain barrier involves perlecan, a heparan sulfate proteoglycan. *J. Neurochem.* **83**, 381–389.

Dobrogowska D. H. and Vorbrodt A. W. (1999) Quantitative immunocytochemical study of blood–brain barrier glucose transporter (GLUT-1) in four regions of mouse brain. *J. Histochem. Cytochem.* **47**, 1021–1030.

Doyle L. A., Yang W., Abruzzo L. V., Krogmann T., Gao Y., Rishi A. K. and Ross D. D. (1998) A multidrug resistance transporter from human MCF-7 breast cancer cells. *Proc. Natl Acad. Sci. USA* **95**, 15665–15670.

Dynon M. K., Jarrott B. and Louis W. J. (1983) Tissue distribution and hypotensive effect of prazosin in the conscious rat. *J. Cardiovasc. Pharmacol.* **5**, 235–239.

Eisenblatter T. and Galla H. J. (2002) A new multidrug resistance protein at the blood–brain barrier. *Biochem. Biophys. Res. Commun.* **293**, 1273–1278.

Eisenblatter T., Huwel S. and Galla H. J. (2003) Characterisation of the brain multidrug resistance protein (BMDP/ABCG2/BCRP) expressed at the blood–brain barrier. *Brain Res.* **971**, 221–231.

Ewart G. D., Cannell D., Cox G. B. and Howells A. J. (1994) Mutational analysis of the traffic ATPase (ABC) transporters involved in uptake of eye pigment precursors in *Drosophila melanogaster*: implications for structure-function relationships. *J. Biol. Chem.* **269**, 10370–10377.

van Herwaarden A. E., Jonker J. W., Wagenaar E., Brinkhuis R. F., Schellens J. H., Beijnen J. H. and Schinkel A. H. (2003) The breast cancer resistance protein (Bcrp1/Abcg2) restricts exposure to the dietary carcinogen 2-amino-1-methyl-6-phenylimidazo[4,5-*b*]pyridine. *Cancer Res.* **63**, 6447–6452.

Hori S., Ohtsuki S., Hosoya K., Nakashima E. and Terasaki T. (2004) A pericyte-derived angiopoietin-1 multimeric complex induces occludin gene expression in brain capillary endothelial cells through Tie-2 activation *in vitro*. *J. Neurochem.* **89**, 503–513.

Hosoya K., Asaba H. and Terasaki T. (2000a) Brain-to-blood efflux transport of estrone-3-sulfate at the blood–brain barrier in rats. *Life Sci.* **67**, 2699–2711.

Hosoya K., Takashima T., Tetsuka K., Nagura T., Ohtsuki S., Takanaga H., Ueda M., Yanai N., Obinata M. and Terasaki T. (2000b) mRNA expression and transport characterization of conditionally immortalized rat brain capillary endothelial cell lines; a new *in vitro* BBB model for drug targeting. *J. Drug Target.* **8**, 357–370.

Hosoya K., Tomi M., Ohtsuki S., Takanaga H., Saeki S., Kanai Y., Endou H., Naito M., Tsuruo T. and Terasaki T. (2002) Enhancement of L-cystine transport activity and its relation to xCT gene induction at the blood–brain barrier by diethyl maleate treatment. *J. Pharmacol. Exp. Ther.* **302**, 225–231.

Imai Y., Nakane M., Kage K., Tsukahara S., Ishikawa E., Tsuruo T., Miki Y. and Sugimoto Y. (2002) C421A polymorphism in the human breast cancer resistance protein gene is associated with low expression of Q141K protein and low-level drug resistance. *Mol. Cancer Ther.* **1**, 611–616.

Jonker J. W., Buitelaar M., Wagenaar E. *et al.* (2002) The breast cancer resistance protein protects against a major chlorophyll-derived

dietary phototoxin and protoporphyria. *Proc. Natl Acad. Sci. USA* **99**, 15649–15654.

Kage K., Tsukahara S., Sugiyama T., Asada S., Ishikawa E., Tsuruo T. and Sugimoto Y. (2002) Dominant-negative inhibition of breast cancer resistance protein as drug efflux pump through the inhibition of S-S dependent homodimerization. *Int. J. Cancer* **97**, 626–630.

Kang Y. S., Ohtsuki S., Takanaga H., Tomi M., Hosoya K. and Terasaki T. (2002) Regulation of taurine transport at the blood–brain barrier by tumor necrosis factor-alpha, taurine and hypertonicity. *J. Neurochem.* **83**, 1188–1195.

Maliepaard M., Scheffer G. L., Faneyte I. F., van Gastelen M. A., Pijnenborg A. C., Schinkel A. H., van De Vijver M. J., Scheper R. J. and Schellens J. H. (2001) Subcellular localization and distribution of the breast cancer resistance protein transporter in normal human tissues. *Cancer Res.* **61**, 3458–3464.

Miwa M., Tsukahara S., Ishikawa E., Asada S., Imai Y. and Sugimoto Y. (2003) Single amino acid substitutions in the transmembrane domains of breast cancer resistance protein (BCRP) alter cross resistance patterns in transfectants. *Int. J. Cancer* **107**, 757–763.

Mogi M., Yang J., Lambert J. F., Colvin G. A., Shiojima I., Skurk C., Summer R., Fine A., Quesenberry P. J. and Walsh K. (2003) Akt signaling regulates side population cell phenotype via Bcrp1 translocation. *J. Biol. Chem.* **278**, 39068–39075.

Mori S., Takanaga H., Ohtsuki S., Deguchi T., Kang Y. S., Hosoya K. and Terasaki T. (2003) Rat organic anion transporter 3 (rOAT3) is responsible for brain-to-blood efflux of homovanillic acid at the abluminal membrane of brain capillary endothelial cells. *J. Cereb. Blood Flow Metab.* **23**, 432–440.

Ohtsuki S., Asaba H., Takanaga H., Deguchi T., Hosoya K., Otagiri M. and Terasaki T. (2002) Role of blood–brain barrier organic anion transporter 3 (OAT3) in the efflux of indoxyl sulfate, a uremic toxin: its involvement in neurotransmitter metabolite clearance from the brain. *J. Neurochem.* **83**, 57–66.

Robey R. W., Honjo Y., van de Laar A., Miyake K., Regis J. T., Litman T. and Bates S. E. (2001) A functional assay for detection of the mitoxantrone resistance protein, MXR (ABCG2). *Biochim. Biophys. Acta* **1512**, 171–182.

Schinkel A. H., Kemp S., Dolle M., Rudenko G. and Wagenaar E. (1993) N-Glycosylation and deletion mutants of the human MDR1 P-glycoprotein. *J. Biol. Chem.* **268**, 7474–7481.

Stewart D. J., Green R. M., Mikhael N. Z., Montpetit V., Thibault M. and Maroun J. A. (1986) Human autopsy tissue concentrations of mitoxantrone. *Cancer Treat. Report* **70**, 1255–1261.

Suzuki M., Suzuki H., Sugimoto Y. and Sugiyama Y. (2003) ABCG2 transports sulfated conjugates of steroids and xenobiotics. *J. Biol. Chem.* **278**, 22644–22649.

Terasaki T., Ohtsuki S., Hori S., Takanaga H., Nakashima E. and Hosoya K. (2003) New approaches to *in vitro* models of blood–brain barrier drug transport. *Drug Discov. Today* **8**, 944–954.

Tetsuka K., Hosoya K., Ohtsuki S., Takanaga H., Yanai N., Ueda M., Obinata M. and Terasaki T. (2001) Acidic amino acid transport characteristics of a newly developed conditionally immortalized rat type 2 astrocyte cell line (TR-AST). *Cell Struct. Funct.* **26**, 197–203.

Zelcer N., Reid G., Wielinga P., Kuil A., van der Heijden I., Schuetz J. D. and Borst P. (2003) Steroid and bile acid conjugates are substrates of human multidrug-resistance protein (MRP) 4 (ATP-binding cassette C4). *Biochem. J.* **371**, 361–367.

Zhang Y., Han H., Elmquist W. F. and Miller D. W. (2000) Expression of various multidrug resistance-associated protein (MRP) homologues in brain microvessel endothelial cells. *Brain Res.* **876**, 148–153.

Zhang W., Mojsilovic-Petrovic J., Andrade M. F., Zhang H., Ball M. and Stanimirovic D. B. (2003) The expression and functional characterization of ABCG2 in brain endothelial cells and vessels. *FASEB J.* **17**, 2085–2087.

Journal of Neurochemistry, 2004, **91**, 1244–1248 doi:10.1111/j.1471-4159.2004.02842.x

RAPID COMMUNICATION

Application of magnetically isolated rat retinal vascular endothelial cells for the determination of transporter gene expression levels at the inner blood–retinal barrier

Masatoshi Tomi and Ken-ichi Hosoya

Faculty of Pharmaceutical Sciences, Toyama Medical and Pharmaceutical University, Sugitani, Toyama, Japan

Abstract

The purpose of the present study was to quantify transporter gene levels at the inner blood–retinal barrier (inner BRB) using a combination of magnetic isolation method for rat retinal vascular endothelial cells (RVEC) and real-time quantitative PCR analysis. The transcript levels of CD31, Tie-2, claudin-5, occludin, Jam-1, mdr1a, oatp2, and oatp14 in the RVEC fraction were more than 100-fold greater than those in the non-RVEC fraction, suggesting that these genes are predominantly expressed at the inner BRB. The transcript levels of GLUT1 and MCT1 in the RVEC fraction were the most abundant in the respective transporter family, suggesting that GLUT1 and MCT1 play a predominant role in D-glucose and monocarboxylate transport, respectively, at the inner BRB. In conclusion, application of magnetically isolated RVEC is able to determine transporter gene levels at the inner BRB thereby increasing our understanding of inner BRB functions at a molecular level.

Keywords: CD31, inner blood–retinal barrier, retinal vascular endothelial cells, magnetic beads coated antibody, transporter.

J. Neurochem. (2004) **91**, 1244–1248.

The inner blood–retinal barrier (inner BRB) forms complex tight junctions of retinal vascular endothelial cells (RVEC) to restrict non-specific transport between the circulating blood and neural retina. Therefore, transporters at the inner BRB play essential roles in supplying nutrients to the retina and are responsible for the efflux of neurotransmitter metabolites from the retina to maintain neural functions. It is important to elucidate the transporter expression and expression levels at the inner BRB in order to understand their physiological roles and design improved systems for drug delivery to the retina. Primary cultured and immortalized RVEC have been used to study transporter expression and transport functions as an *in vitro* model of the inner BRB (Greenwood 1992; Hosoya *et al.* 2004; Nakashima *et al.* 2004). Although it is easy to carry out transport studies and measure the mRNA expression of transporters by RT-PCR analysis, there is no way of knowing whether transporter expression levels are changed by culture passages and conditions. Immunohistochemical analysis and *in situ* hybridization have been used to identify transporter protein and mRNA, respectively, at the inner BRB *in vivo* (Gerhart *et al.* 1999; Gao *et al.* 2002). However, there are some limitations in studying the quantification of transporters due to the complexity of the method and its poor sensitivity.

It is thought that isolation of RVEC simplifies the investigation of the gene expression profile at the inner BRB *in vivo*. Nevertheless, this technique has not been applied to the quantification of transporters. It is difficult to obtain enough purified RVEC as RVEC represents a small percentage of the weight of the entire retina and the retina itself is a very small tissue. The cell surface antigen CD31 (platelet-endothelial cell adhesion molecule-1; PECAM-1) is exclusively and extensively expressed on the membrane of endothelial cells (Scholz and Schaper 1997). Therefore, magnetic beads coated with anti-CD31 antibodies are able to collect highly purified endothelial cells from a tissue homogenate using a magnet (Demeule *et al.* 2001). Su *et al.* (2003) applied this technique to establish primary cultured mouse RVEC and obtained an RVEC purity of almost 100%, as determined by two endothelial markers and FACS analysis. Quantitative real-time PCR analysis means that mRNA levels can be quantified in a very sensitive manner. Therefore, a combination of magnetic isolation of highly purified RVEC and quantitative real-time PCR analysis allows the determination of transporter mRNA levels at the inner BRB *in vivo*. This is an important method which allows us to examine the molecular levels of transporters at the inner BRB, in addition to *in vitro* and *in vivo* functional transport studies.

The purpose of the present study was to isolate rat RVEC using magnetic beads coated with anti-rat CD31 antibodies, and quantify the transcript level of endothelial markers, tight junction proteins, and transporters at the inner BRB.

Materials and methods

Animals

Male Wistar rats, weighing 250–300 g, were purchased from SLC (Shizuoka, Japan). The investigations using rats described in this report conformed to the provisions of the Animal Care Committee, Toyama Medical & Pharmaceutical University (# 2003–48) and the ARVO Statement on the Use of Animals in Ophthalmic and Vision Research.

Received August 3, 2004; revised manuscript received August 25, 2004; accepted August 26, 2004.

Address correspondence and reprint requests to K. Hosoya, Faculty of Pharmaceutical Sciences, Toyama Medical and Pharmaceutical University, 2630, Sugitani, Toyama, 930–0194, Japan. E-mail: hosoyak@ms.toyama-mpu.ac.jp

Abbreviations used: BRB, blood–retinal barrier; CRT, creatine transporter; GLUT, glucose transporter; MCT, monocarboxylate transporter; mdr, multidrug resistance protein; oatp, organic anion transporting polypeptide; RVEC, retinal vascular endothelial cells; SM, smooth muscle.

Isolation of RVEC

RVEC isolation was performed using a modification of the procedure described by Su *et al.* (2003) with affinity purification using magnetic beads coated with anti-rat CD31 antibodies. Mouse anti-rat CD31 antibodies (Chemicon, Temecula, CA, USA) were incubated with Dynabeads pan mouse IgG (Dynal Biotech, Lake Success, NY, USA) overnight at 4°C to prepare magnetic beads coated with anti-rat CD31 antibodies. Rat retinas were minced and digested in 0.1% collagenase type I (Invitrogen, Carlsbad, CA, USA) and 0.01% DNase I (Roche, Mannheim, Germany) in Ca^{2+}- and Mg^{2+}-free Hank's balanced salt solution (HBSS) for 30 min at 37°C with agitation. Digests were filtered through a 30 μm nylon mesh, and then centrifuged at 200 × *g* for 10 min. The pellets were resuspended in Dulbecco's modified Eagle's medium containing 10% fetal bovine serum and incubated with magnetic beads coated with anti-rat CD31 antibodies for 1 h at room temperature. RVEC labeled with the magnetic beads were positively selected by affinity binding to the magnet.

Quantitative real-time PCR analysis

Quantitative real-time PCR was performed using an ABI PRISM 7700 sequence detector system (PE-Applied Biosystems, Foster City, CA, USA) with 2X SYBR Green PCR Master Mix (PE-Applied Biosystems) as described in a previous report (Hosoya *et al.* 2004) and gene specific primers (Table 1) through 40 cycles of 94°C for 30 s, 55–60°C for 30 s, and 72°C for 1 min. A standard curve was generated for each run using variety amounts of the plasmid containing the target gene. This enabled to quantify the initial copy number of target mRNA in the samples despite the different PCR condition of target genes. Each mRNA expression level was normalized with respect to the β-actin mRNA expression.

Results and discussion

Endothelial markers

In order to isolate RVEC from the retinal homogenate, magnetic beads coated with anti-rat CD31 antibodies were used and the magnetically collected and non-collected cells were isolated as RVEC and non-RVEC fractions, respectively. Endothelial specific markers, such as CD31 (Scholz and Schaper 1997) and Tie-2, endothelial specific receptor tyrosine kinase, were first analyzed to confirm for concentration of RVEC (Table 2). The transcript level of CD31 in the RVEC fraction was 270-fold greater than that in the non-RVEC fraction. Moreover, the expression of Tie-2 mRNA was only detected in the RVEC fraction, and not in the non-RVEC fraction. Claudin-5 and occludin are exclusively localized at the inner BRB to form tight junction strands (Morcos *et al.* 2001; Barber and Antonetti 2003). Junctional adhesion molecule-1 (Jam-1) also takes part in the formation of tight junctions, together with claudin-5 and occludin. The transcript level of claudin-5, occludin and Jam-1 in the RVEC fraction was 2,830-, 106-, and 127-fold greater, respectively, than that in the non-RVEC fraction. These results suggest that RVEC in the RVEC fraction is concentrated more than 100-fold compared with the non-RVEC fraction.

Non-endothelial markers

Glial cells markers, such as S-100β and glutamine synthetase, and a neuronal marker of neurofilament heavy chain were examined in the RVEC fraction (Table 2). The transcript level of S-100β, glutamine synthetase, and neurofilament heavy chain in the RVEC fraction was 7.3–33-fold less than that in the non-RVEC fraction, suggesting that less than 10% of the RVEC fraction is the glial and neuronal cells. In the case

Table 1 Oligonucleotide primers used for PCR amplification of cDNAs

Target mRNA	Accession Number	Upstream primer (5′ to 3′)	Downstream primer (5′ to 3′)	Product size
CD31 (PECAM-1)	RNU77697	CTT CAC CAT CCA GAA GGA AGA GAC	CAC TGG TAT TCC ATG TCT CTG GTG	360 bp
Tie-2	NM_013690*	GGG CAA AAA TGA AGA CCA GCA C	GCA TCC ATC CGT AAC CCA TCC T	516 bp
Claudin-5	XM_344058	GCA GAG CAC CGG GCA CAT GC	TAG TTC TTC TTG TCG TAA TCG CC	483 bp
Occludin	NM_031329	GCC TTT TGC TTC ATC GCT TCC	AAC AAT GAT TAA AGC AAA AGC CAC	351 bp
Jam-1	NM_053796	ACA GCC ATG AGG TCA GAG GCT	ACC TAG AAG ACA TTG AAG GCA TC	348 bp
S-100β	NM_013191	ATG TCT GAG CTG GAG AAG GCC	TCA CTC ATG TTC AAA GAA CTC ATG	279 bp
Glutamine synthetase	NM_017073	TAC CCG AGT GGA ACT TTG ATG	TAA AGT TGG TGT GGC AGC CTG	600 bp
Neurofilament heavy chain	NM_012607	TTG GAC CGA CTC TCA GAG GCA G	CAA TCC GAC ACT CTT CGC CTT CC	352 bp
α-Smooth muscle actin	X06801	TAT GTG TGA AGA GGA AGA CA	CAC AAT ACC AGT TGT ACG TC	463 bp
mdr1a (Abcb1a)	NM_133401	ACA GAA ACA GAG GAT CGC	CGT CTT GAT CAT GTG GCC	437 bp
mdr1b (Abcb1b)	NM_012623	ACA GAA ACA GAG GAT CGC	AGA GGC ACC AGT GTC ACT	352 bp
mdr2 (Abcb4)	NM_012690	ACA GAA ACA GAG GAT CGC	ATG CGT GCT TTC CAG CCA	384 bp
GLUT1 (Slc2a1)	NM_138827	GAT GAT GAA CCT GTT GGC CT	AGC GGA ACA GCT CCA AGA TG	503 bp
GLUT3 (Slc2a3)	NM_017102	GAC GAG AGT ATC AGG ATG TCA CAG	AGG CCA CGT AGA CCA AGA TAG CC	397 bp
GLUT4 (Slc2a4)	NM_012751	GTT ATG TGT CCA TCG TGG CCA TAT	CAG TCA TTC TCA TCT GGC CCT AAG	388 bp
MCT1 (Slc16a1)	NM_012716	GAA AAA CTC AAG TCC AAA GAG TCT	TTT CAT TGT CTT CTT GGG CTT CT	801 bp
MCT2 (Slc16a7)	NM_017302	CCT CTG CCC CCT AGC CCA TT	TCT GAG GGA GGA TTG TGT GTA TT	447 bp
Oatp1 (Slc21a1)	NM_017111	AAG GCC ATG AAC AGA ATG CAC ACT	AGA AAC AGG AAA TGA CAC AGG AGT GA	548 bp
Oatp2 (Slc21a5)	NM_131906	TAC TGC CCT ATG CAA GGC CAT GAA	AAC TAA CGC AAT CTG GCT TAA CCA A	397 bp
Oatp3 (Slc21a7)	NM_030838	CGC TTG GGA TTG GAT TAC ATG CAT	ATG AGA CAG TGG CCT TTG GAG AAT	612 bp
Oatp14 (Slc21a14)	NM_053441	CCT GGT GGC TTG GTT ACC TAA TAG	CTG CCC ATA CTG CTG CTC AAT GT	344 bp
CRT (Slc6a8)	NM_017348	GAA ATG GTG CTG GTC CTT CTT CAC	GTC ACA TGA CAC TCT CCA CCA CGA	353 bp
β-Actin	NM_031144	TCA TGA AGT GTG ACG TTG ACA TCC GT	CCT AGA AGC ATT TGC GGT GCA CGA TG	285 bp

*Represents the mouse sequence (the rat sequence has not been reported).